JOURNAL OF GEOPHYSICAL RESEARCH, VOL. 98, NO. B5, PAGES 7887–7902, MAY 10, 1993

Chemical Variation Trends at Fast and Slow Spreading Mid-Ocean Ridges

YAOLING NIU[1] AND RODEY BATIZA

Department of Geology and Geophysics, University of Hawaii at Manoa, Honolulu

We examined an expanded global data set of mid-ocean ridge basalt (MORB) major element analyses. In agreement with previous results, we show that slow spreading ridges tend to have more primitive (high Mg/Fe) lavas than fast spreading ridges. Fractionation-corrected values of $Na_{(8)}$ and $Ca_{(8)}/Al_{(8)}$ (indices of the extent of melting) and $Si_{(8)}/Fe_{(8)}$ (an index of the pressure of melting) do not vary systematically with spreading rate. Assuming a mantle that is generally homogeneous in major elements, we conclude that average mantle temperature in the region of melting below mid-ocean ridges is independent of spreading rate. Using data for 32 best sampled ridge segments of variable length, we show that the so-called global and local trends of chemical variation (Klein and Langmuir, 1989) are systematically distributed with spreading rate. The global trend (positive correlation between extent of melting and melting pressure) occurs at fast spreading ridges (> 60 mm/yr), while the local trend (negative correlation between extent of melting and melting pressure) occurs at slow spreading ridges (< 50 mm/yr). This distribution is independent of geographic length scale. Among the 32 ridge systems we examined, the slopes of the two trends on chemical diagrams show some variability, but no regular pattern, such as fanning. The global trend is well-explained by differences in average mantle temperature occurring at several length scales within mantle rising passively in response to plate separation. We propose that the local trend arises from processes occurring in buoyant diapirs undergoing melting and melt-solid reequilibration. Several lines of geophysical and geological evidence point to the importance of buoyant, three-dimensional mantle upwelling beneath slow spreading ridges. Petrologic modeling presented here is consistent with this hypothesis, as is the existence of the local trend at seamounts on the flanks of the East Pacific Rise.

INTRODUCTION

Spreading rate is an important variable associated with many significant differences along the global mid-ocean ridge system. For example, morphologic differences are largely controlled by spreading rate [e.g., *Macdonald*, 1982; *Franchteau and Ballard*, 1983], with slow spreading ridges typically having deep axial rift valleys that are much less pronounced or are absent at fast spreading rates. Related topographic roughness on the flanks of mid-ocean ridges also depends on spreading rate [*Malinverno and Pockalny*, 1990; *Malinverno*, 1991; *Hayes and Kane*, 1991; *Small and Sandwell*, 1989]. Along-axis gravity [*Lin et al.*, 1990; *Lin and Phipps Morgan*, 1992] shows important changes with spreading rate, interpreted to reflect fundamental differences in the style of mantle upwelling, with dominantly two-dimensional, plate-driven upwelling below fast spreading ridges and more three-dimensional buoyantly driven, diapiric upwelling beneath slow spreading ridges [*Parmentier and Phipps Morgan*, 1990].

In addition to topographic and geophysical differences, petrologic differences exist between fast and slow spreading ridges [*Morel and Hekinian*, 1980; *Natland*, 1980; *Flower*, 1980; *Batiza*, 1991; *Sinton and Detrick*, 1992] with slow spreading ridges typically having more primitive (higher Mg/Fe) lavas and fast spreading ridges having more fractionated ones. Relationships between isotopic variability and spreading rate [*Cohen and O'Nions*, 1982; *Hamelin and Allègre*, 1985; *Batiza*, 1984] are more controversial [*Ito et al.*, 1987; *Holness and Richter*, 1989].

In this study, we examine an expanded global data set of mid-ocean ridge basalt (MORB) major element analyses. In agreement with previous studies, we find that fast spreading ridges have, on average, more fractionated, lower Mg/Fe MORB lavas than slow spreading ridges. We then use data for 32 well-sampled portions of the global ridge system to evaluate chemical variation trends as a function of plate spreading rate. *Klein and Langmuir* [1987] showed that globally, MORB shows an inverse correlation between $Fe_{(8)}$ and $Na_{(8)}$, where the subscript denotes values corrected for shallow fractionation to an MgO content of 8.0 wt %. They interpreted this in terms of a polybaric decompression melting model and showed that deep (high $Fe_{(8)}$), extensive (low $Na_{(8)}$) melting would be expected from the pooling of polybaric melts produced from a long mantle column with high initial melting temperature. In contrast, a short mantle melting column with low initial melting temperature would be expected to produce pooled melts reflecting shallower (low $Fe_{(8)}$) and less extensive (high $Na_{(8)}$) melting. Regionally averaged MORB analyses exhibit a trend of negative correlation between $Fe_{(8)}$ and $Na_{(8)}$ called the global trend by *Klein and Langmuir* [1989].

However, some mid-ocean ridge segments, such as the mid-Atlantic ridge at 26°S [*Batiza et al.*, 1988], exhibit an opposite trend: $Fe_{(8)}$ and $Na_{(8)}$ show a positive, not inverse correlation. That is, shallow (low $Fe_{(8)}$), extensive (low $Na_{(8)}$) melting is on a trend with deep (high $Fe_{(8)}$), less extensive (high $Na_{(8)}$) melting. This trend of chemical variation was termed the local trend by *Klein and Langmuir* [1989]. The global and local trends are shown in Figure 1.

In this study, we find that the so-called global trend is found at fast (> 60 mm/yr) spreading ridges and that the so-called local trend is found at slow (< 50 mm/yr) spreading ridges. Transitional ridges (50 - 60 mm/yr) may exhibit either trend of chemical variation. This finding is independent of the ridge length and thus, the terms "global" and "local" are not particularly apt. Even so, we retain the previous usage of these

[1]Now at Lamont-Doherty Earth Observatory, Palisades, New York.

Paper number 93JB00149.
0148–0227/93/93JB–00149$05.00

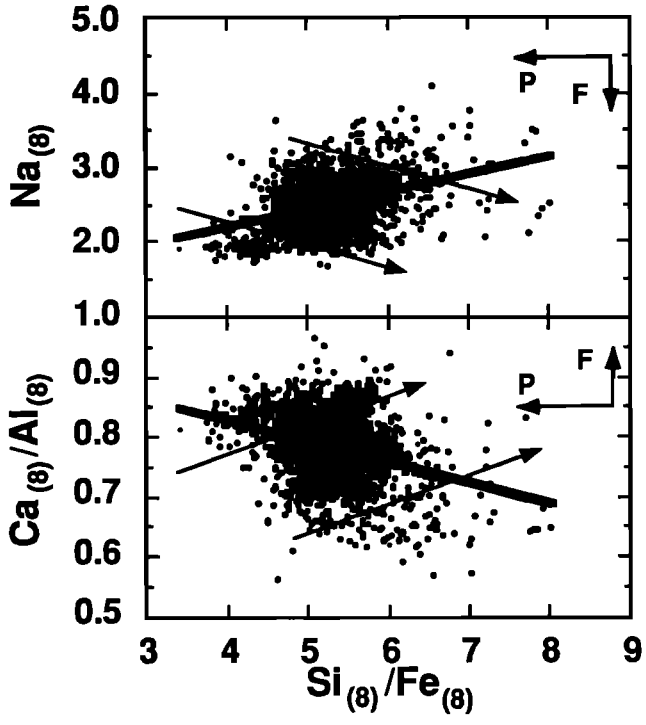

Fig. 1. The global and local trends of chemical variation [*Klein and Langmuir*, 1989] are shown here on $Na_{(8)}$ and $Ca_{(8)}/Al_{(8)}$ versus $Si_{(8)}/Fe_{(8)}$. The subscript denotes values of the oxide corrected for shallow fractionation to a MgO content of 8.0 wt % [*Klein and Langmuir*, 1987]. Following *Niu and Batiza* [1991*a*], we use both $Na_{(8)}$ and $Ca_{(8)}/Al_{(8)}$ as indices of the extent of melting and $Si_{(8)}/Fe_{(8)}$ as an index of the pressure of melting. Arrows on each diagram point to high pressure and higher extent of melting. The data points are from our new global data set of MORB. The heavy line shows the so-called global trend, and the thin solid lines with arrows show (schematically) examples of local trends.

terms in this paper. We consider several possible origins for the local trend and conclude that it is due to fundamental differences in the dynamics of mantle upwelling and melt segregation beneath slow and fast spreading ridges.

THE DATA SET

To the data set of *Brodholt and Batiza* [1989], we have added the data of *Sinton et al.* [1991] for the southern East Pacific Rise (EPR), *Thompson et al.* [1989] and *Hekinian et al.* [1989] for the northern EPR, *Klein et al.* [1991] and *Dosso et al.* [1988] for the South-East Indian ridge, *Humler and Whitechurh* [1988] for the Central Indian ridge, *Michael et al.* [1989] for the Explorer ridge, and *Bougault et al.* [1988] for the northern Mid-Atlantic Ridge (MAR). We also use the updated version of *Melson and O'Hearn's* [1986] Smithsonian Volcanic Glass Project (SIVGP) data base (W. G. Melson and T. O'Hearn, personal communication, 1991). We use sample group means for our analysis and include both glass and whole rock data. Using correction factors of *Batiza and Niu* [1992], we adjust Lamont-Doherty Earth Observatory and University of Hawaii glass probe analyses to conform with the Smithsonian analyses. Data sources of MORB analyses are given in Table 1.

Spreading rates are from NUVEL 1 [*DeMets et al.*, 1990] except for the Explorer ridge [*Botros and Johnson*, 1988], Juan de Fuca [*Wilson*, 1988] and Gorda ridge [*Davis and Clague*, 1987].

RESULTS

Oxide Trends With Spreading Rate

Plots of the global MORB data against spreading rate show much scatter but statistically significant trends for most of the major and minor elements, confirming previous findings that lavas from fast spreading ridges are typically more fractionated than those erupted at slow spreading ridges. With increasing spreading rate, TiO_2, FeO, Na_2O, and P_2O_5 increase, while Al_2O_3, MgO, and CaO decrease. The exceptions are SiO_2 and K_2O. SiO_2 may show no trend because of analytical problems discussed by *Klein and Langmuir* [1989]. K_2O, on the other hand, shows a significant correlation with spreading rate, but it is inconsistent with a fractionation. This is because K is a very incompatible element and is very sensitive to mantle source heteroheneity; higher K_2O contents in MORBs at slow spreading rate obviously result from hot spot effect such as at the North Atlantic ridge. Table 2 gives the slopes, intercepts, and correlation coefficients of these linear trends, and Figure 2 shows representative examples. When the analyses are corrected for shallow fractionation (see notes to Table 2 and *Niu* [1992] for correction procedure), these correlations virtually disappear. As shown in Table 2 and Figure 2, after correction, the slopes are reduced by at least an order of magnitude; plots of chemical variations against spreading rate are essentially flat (with much scatter).

Assuming a homogeneous mantle source and a column melting model similar to that of *Klein and Langmuir* [1987], we next plot indices of the extent of melting and depth of melting against spreading rate (Figure 3). $Si_{(8)}/Fe_{(8)}$ is a very sensitive indicator of the pressure of melting [*Niu and Batiza*, 1991*a*] and $Na_{(8)}$and $Ca_{(8)}/Al_{(8)}$ are good indices of the extent of partial melting of pooled column melts [*Klein and Langmuir*, 1987; *Niu and Batiza*, 1991*a*]. As shown in Figure 3, plots of these quantities against spreading rate exhibit much scatter. There is a suggestion that the scatter is more pronounced at slow spreading rates. This, as will be discussed later, is associated with the so-called local trend at slow spreading ridges. Nevertheless, there is no evidence for systematic trends in either depth of melting or extent of melting with differences in spreading rate. This is an interesting finding because it confirms that average mantle temperature, an important control on melting below ridges [*McKenzie*, 1984; *Klein and Langmuir*, 1987; *McKenzie and Bickle*, 1988], is variable, but essentially independent of spreading rate [*Klein and Langmuir*, 1987].

Chemical Variation Trends Versus Spreading Rate

Next, we searched the global data set for spreading-rate dependence in MORB chemical variation trends. As shown by *Klein and Langmuir* [1987], regionally averaged MORB data exhibit correlations among axial depth, inferred extent of melting and inferred depth of melting. Unaveraged raw data exhibit similar trends [*Brodholt and Batiza*, 1989], such that deeper melts (high $Fe_{(8)}$, low $Si_{(8)}/Fe_{(8)}$) are formed by higher extents of melting (low $Na_{(8)}$ and high $Ca_{(8)}/Al_{(8)}$). Similarly, shallower melts (low $Fe_{(8)}$, high $Si_{(8)}/Fe_{(8)}$) are formed by lower extents of melting (higher $Na_{(8)}$). This behavior, observed globally, was called the global trend [*Klein and Langmuir*, 1989]. The opposite trend, with a positive correlation between $Fe_{(8)}$ and $Na_{(8)}$, was noted by *Batiza et al.* [1988] and *Brodholt and Batiza* [1989] and called the local trend by *Klein and Langmuir* [1989]. Here, we try to determine whether the

TABLE 1. Data Set

Ridge	Group Means	MgO>5wt %	Data Sources
North EPR	553	531	1,4,6,11,23,24,25,26,30,35,42,43,54,55,56
South EPR	263	243	1,12,45,51,55
Gorda	28	28	1,16
Juan de Fuca	184	181	1,19,31,32
Explorer	87	83	1,15,41
Galapagos	172	130	1,2,13,14,21,22,46,47
Easter, East Ridge	15	15	1,49
Easter, West Ridge	40	40	1,49
North MAR	712	704	1,7,8,9,29,34,40,43,44,48,50,52
South MAR	97	89	1,5,17,28,39,56
Cayman Rise	26	26	1,53
Carlsberg	10	10	1
Red Sea	19	18	1
America-Antarctic	46	46	1,38
SW Indian	39	39	1,20,36,37
SE Indian	63	63	1,3,18,33
Central Indian	33	33	1,27
Total	2387	2279	

1, Smithsonian; 2, *Anderson et al.* [1975]; 3, *Anderson et al.* [1980]; 4, *Batiza and Niu* [1992]; 5, *Batiza et al.* [1988]; 6, *Bender et al.* [1984]; 7, *Bougault and Hekinian* [1974]; 8, *Bougault et al.* [1988]; 9, *Bryan and Moore* [1977]; 10, *Bryan* [1979]; 11, *Byers et al.* [1986]; 12, *Campsie et al.* [1984]; 13, *Christie and Sinton* [1986]; 14, *Clague et al.* [1981]; 15, *Cousens et al.* [1984]; 16, *Davis and Clague* [1987]; 17, *Dickey et al.* [1977]; 18, *Dosso et al.* [1988]; 19, *Eaby et al.* [1984]; 20, *Engel and Fisher* [1975]; 21, *Fisk et al.* [1982]; 22, *Perfit et al.* [1983]; 23, *Hawkins and Melchior* [1980]; 24, *Hekinian and Walker* [1987]; 25, *Hekinian et al.* [1985]; 26, *Hekinian et al.* [1989]; 27, *Humler and Whitechurch* [1988]; 28, *Humphris et al.* [1985]; 29, *Jakobsson et al.* [1978]; 30, *Juteau et al.* [1980]; 31, *Karsten* [1988]; 32, *Karsten et al.* [1990]; 33, *Klein et al.* [1991]; 34, *Langmuir et al.* [1977]; 35, *Langmuir et al.* [1986]; 36, *Le Roex et al.* [1982]; 37, *Le Roex et al.* [1983]; 38, *Le Roex et al.* [1985]; 39, *Le Roex et al.* [1987]; 40, *Melson and O'Hearn* [1986]; 41, *Michael et al.* [1989]; 42, *Moore et al.* [1977]; 43, *Morel* [1979]; 44, *Neumann and Schilling* [1984]; 45, *Renard et al.* [1985]; 46, *Schilling et al.* [1976]; 47, *Schilling et al.* [1982]; 48, *Schilling et al.* [1983]; 49, *Schilling et al.* [1985]; 50, *Sigurdsson* [1981]; 51, *Sinton et al.* [1991]; 52, *Stakes et al.* [1984]; 53, *Thompson et al.* [1980]; 54, *Thompson et al.* [1989]; 55, *Tighe* [1988] (EPR synthesis); 56, unpublished data of Batiza and Niu.

TABLE 2. Global Correlations

	Raw Data				Corrected for Fractionation*		
	Slope	Intercept	R		Slope	Intercept	R
SiO_2	7.45×10^{-4}	50.65	2.63×10^{-2}	$Si_{(8)}$	-2.18×10^{-3}	50.52	1.45×10^{-1}
TiO_2	3.84×10^{-3}	1.39	3.73×10^{-1}	$Ti_{(8)}$	6.96×10^{-4}	1.31	1.42×10^{-1}
Al_2O_3	-7.14×10^{-3}	15.30	3.12×10^{-1}	$Al_{(8)}$	-2.60×10^{-3}	15.63	1.87×10^{-1}
FeO	8.87×10^{-3}	9.98	2.51×10^{-1}	$Fe_{(8)}$	-2.04×10^{-3}	9.70	1.04×10^{-1}
MgO	-6.43×10^{-3}	7.65	2.55×10^{-1}		-	-	-
CaO	-4.17×10^{-3}	11.70	1.79×10^{-1}	$Ca_{(8)}$	1.04×10^{-3}	11.99	7.09×10^{-2}
Na_2O	2.40×10^{-3}	2.51	2.61×10^{-1}	$Na_{(8)}$	8.81×10^{-4}	2.45	1.19×10^{-1}
K_2O	-4.74×10^{-4}	0.21	1.33×10^{-1}	$K_{(8)}$	-8.89×10^{-4}	0.20	3.11×10^{-1}
P_2O_5	5.22×10^{-4}	0.14	2.84×10^{-1}	$P_{(8)}$	2.11×10^{-4}	0.13	1.64×10^{-1}
				$Si_{(8)}/Fe_{(8)}$	5.85×10^{-4}	5.27	5.12×10^{-2}
				$Ca_{(8)}/Al_{(8)}$	2.00×10^{-4}	0.77	1.63×10^{-1}

* The correction procedure we used [*Niu*, 1992] is similar to the one by *Klein and Langmuir* [1987] with following differences: We use a general polynomial equation that allows to correct every oxide and to use all the samples with MgO ≥ 5.0 wt %. This general equation accounts for the curvature of variation trends in the region of MgO = 9–7 wt %. We corrected all oxides to MgO = 8.0 wt %. The corrected oxide values sum to 100±1%, and plots of corrected oxide values against MgO show essentially zero slope, suggesting that our correlation procedure does not introduce any artifacts. We also apply a regional correction to data from each major geographic area as listed in Table 1 (see *Niu* [1992] for correction coefficients). Values of $R > 0.081$ are significant at 99% confidence level (F test for N = 2387: 99% confidence at $F = 6.63$). $Si_{(8)}/Fe_{(8)}$, $Ca_{(8)}/Al_{(8)}$, and $Na_{(8)}$ values are for the trends shown in Figure 3.

distribution of the global and local trends is systematic with spreading rate.

To do so, we select the 32 best sampled portions of the ridge system from the global data set and examine the data from each area in detail. These are listed in order of increasing spreading rate in Table 3, which also gives the endpoints of each ridge segment, its length, spreading rate, number of chemical group means and sample density. The lengths of these ridge portions vary greatly (Table 3), and all have transforms or nontransform discontinuities or large overlapping spreading centers (OSCs) [*Macdonald et al.*, 1988] as endpoints. Sampling density also varies greatly with the poorest-sampled ridge having ~ 0.7

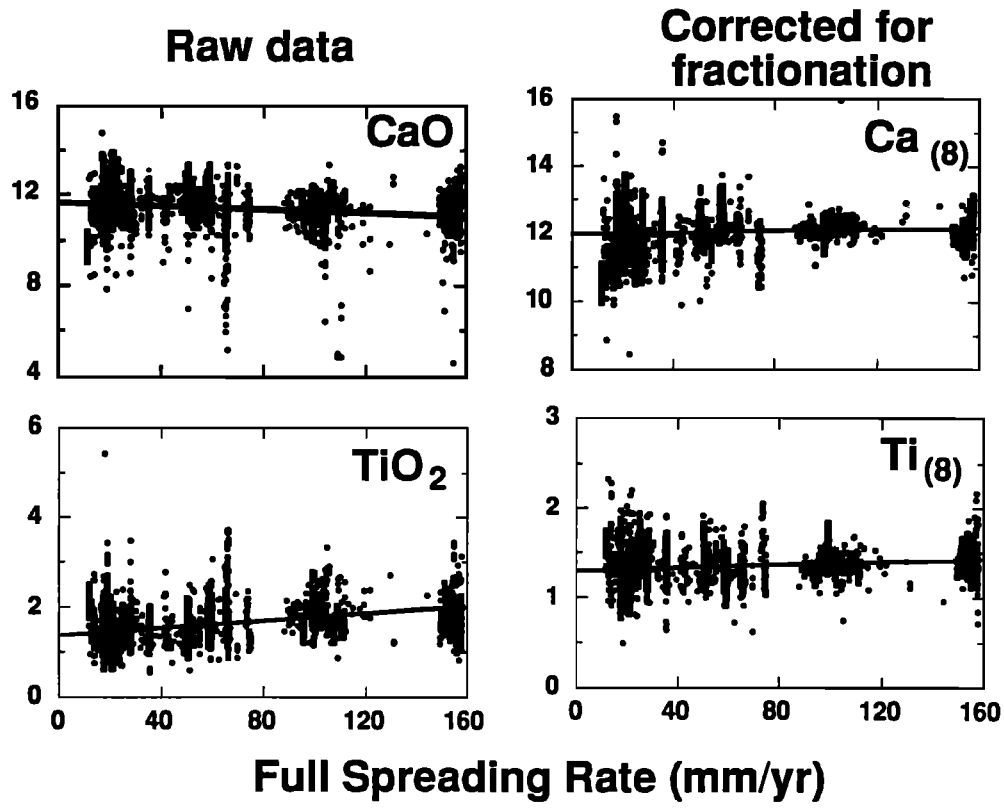

Fig. 2. Examples of the correlation between major element variation and full spreading rate. These correlations are consistent with increasing degrees of low pressure fractionation with increasing spreading rate, as shown by the absence of trends in plots of fractionation corrected data. See Table 2 for data on other major elements.

samples - 10 km^{-1}. Ideally, one would choose ridge segments of comparable length and sampling density; however, the present sample distribution makes this impossible. Another consequence of incomplete sampling is that our group of 32 best sampled areas does not include any portion of the Indian Ocean ridge system (Figure 4). Figure 1 shows plots of $Na_{(8)}$and $Ca_{(8)}/Al_{(8)}$ (indices of extent of melting) against $Si_{(8)}/Fe_{(8)}$ (an index of pressure of melting) for our entire data set. Figure 5 shows the same two plots for each of the 32 individual ridge portions of Table 3.

Most of the 32 ridge segments show clear linear trends with slopes indicative of either the global or local trend. However, some segments show less clear trends, either intrinsically or because of low sampling density. In order to objectively assess how closely the data from each area match the global or local trend, we developed a method for assigning a numerical score to each segment. The scores are derived from (1) the slope and significance (F test) of the regression lines (positive or negative values of the correlation coefficient R); (2) The value and significance (t test) of the correlation coefficients; and (3) sampling density. By this method, areas with very clear trends (little scatter and many samples) receive the highest numerical values (see Table 3, negative score for local trend and positive scores for global trend) and areas with scattered trends and/or fewer samples receive low numerical scores. Details of the scoring procedure are given in the appendix.

Table 3 and Figure 6 summarize the results and show clearly that MORB chemical systematics (local versus global trend) are related to spreading rate. Fast ridges (> 60 mm/yr) exhibit the global trend whereas slow spreading ridges (< 50 mm/yr) exhibit the local trend. Furthermore, this relationship is apparently independent of geographic length scale as Table 3 has ridge segments of highly variable length. For example, at slow spreading rates, both Narrowgate (34.2 km long) and the entire Mid-Atlantic Ridge south of the Kane Fracture Zone (885 km long) exhibit very clear local trends. At fast spreading rates, both small segments and the entire northern and southern EPR exhibit the global trend, as shown previously by *Niu and Batiza* [1991*a*] and *Klein and Langmuir* [1989]. The distribution of these chemical variation trends is thus apparently controlled by spreading rate and not spatial scale, as implied by the terms global and local.

Another important result from Table 3 and Figure 5 is that the slopes of the regression lines for the global and local trends are not constant. Furthermore, as can be seen on Figure 7, the individual regression lines do not exhibit a systematic pattern (such as fanning) on the plots. One possibility is that this variability in slope is due to uncertainty in the slope of the regression lines (data scatter); however, we find no relationship between the correlation coefficients and the slope of the regression lines. Thus it is more likely that this slope variation is real and reflects characteristics of the natural processes that result in the chemical systematics of both fast and slow spreading ridges. Interestingly, there appears to be more clustering of global trends than of local trends.

DISCUSSION

If we assume that the mantle is approximately homogeneous, at least for major elements, then the results of

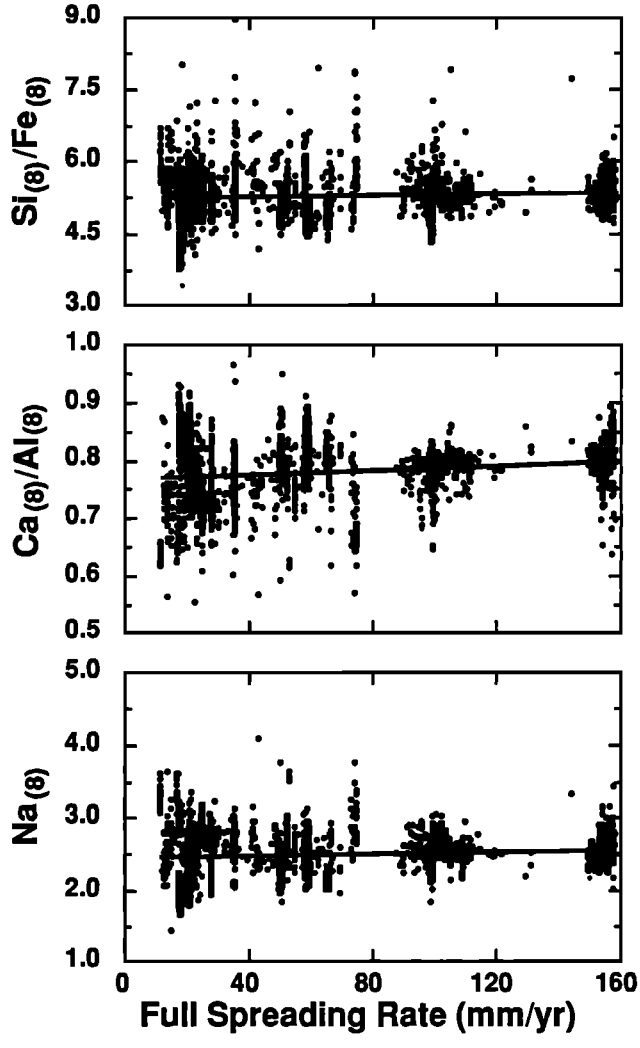

Fig. 3. Variations of $Si_{(8)}/Fe_{(8)}$, $Na_{(8)}$, and $Ca_{(8)}/Al_{(8)}$ as a function of spreading rate. Note that there appears to be greater dispersion at slow spreading rates but that values are essentially constant (and scattered) with spreading rate.

Figure 3 indicate that average mantle temperature is independent of spreading rate. However, chemical variation trends involving pressure and extents of melting do appear to be related to spreading rate (Table 3 and Figures 5 and 6). These trends, the global and local chemical variation trends, appear to be independent of geographic length scale along axis, and the slopes of the trends are variable (Figure 7). These observations suggest strongly that the dynamics of mantle upwelling, thought to differ fundamentally between fast and slow spreading ridges [e.g., *Parmentier and Phipps Morgan*, 1990; *Lin and Phipps Morgan*, 1992; *Scott and Stevenson*, 1989], may play a role in controlling the distribution of the global and local chemical trends in MORB. We hypothesize that the global trend results from melting under conditions dominated by passive, plate driven mantle upwelling that is broadly two-dimensional in character [e.g., *Phipps Morgan*, 1987]. In contrast, the local trend would be the result of melting that occurs in rising mantle dominated by buoyant, three-dimensional upwelling [e.g., *Sotin and Parmentier*, 1989; *Scott and Stevenson*, 1989]. Such buoyant instabilities could be embedded within a mean upward plate-driven flow [*Scott and Stevenson*, 1989]. In fact, since the global trend includes regionally averaged data for many slow spreading ridges, it seems likely that passive upwelling of mantle is also important at slow spreading ridges.

There exists strong evidence from crustal thickness and MORB chemical data [*Klein and Langmuir*, 1987], theoretical considerations [*McKenzie*, 1984], and models of MORB melting [*Klein and Langmuir*, 1987; *McKenzie and Bickle*, 1988; *Niu and Batiza*, 1991*a*] that the global trend of MORB is due principally to differences in average mantle temperature. Hot mantle rising adiabatically intersects the solidus at a deeper level than cooler mantle and continued decompression melting with matrix compaction should result in pooled melts with chemical signatures of high pressure (high $Fe_{(8)}$ and low $Si_{(8)}/Fe_{(8)}$) and high extents of melting (low $Na_{(8)}$ and high $Ca_{(8)}/Al_{(8)}$). Regional differences in mantle temperature should give rise to ensembles of data which exhibit the global trend. Mantle temperature differences of about 200°C are capable of producing the global array [*Klein and Langmuir*, 1987]. On a smaller geographic length scale, differences in mantle temperature can give rise to the same global systematics at a more local or regional level, as shown by *Niu and Batiza* [1991*a*]. Thus this explanation of global trend is fully consistent with both petrological evidence and models of mantle flow beneath fast spreading ridges [e.g., *Lin and Phipps Morgan*, 1992].

The global trend is well-explained by adiabatic decompression melting of a mantle column in which polybaric melts are efficiently separated from their residues and pooled in a reservoir at low pressure [*Klein and Langmuir*, 1987; *Niu and Batiza*, 1991a]. However, in rising diapirs, separation of melt from residue may be less efficient. Whereas rapid melt segregation in a melting column of global trend preserves high-pressure signatures (low $Si_{(8)}/Fe_{(8)}$) at high extents of melting [*Klein and Langmuir*, 1987], extensive melts of the local trend have low-pressure signatures (high $Si_{(8)}/Fe_{(8)}$). One possible explanation is that slow melt segregation in diapirs allows matrix-melt reaction during ascent, such that high pressure signatures are only preserved in melts produced by low extents of melting shortly after initiation of a diapiric instability.

During ascent of a mantle diapir undergoing melting, inefficient melt segregation would allow melts to reequilibrate with the solid matrix. If these reequilibrated melts were tapped by dikes [*Nicolas*, 1986; *Sleep*, 1988] at various pressures, an ensemble of melts resembling the local trend would result. Deep melts would be produced by small extents of melting soon after initiation of the diapir. If these melts are tapped by dikes, they will have chemical signatures of high pressure and low extents of melting. With continued diapiric ascent, melting and melt-solid reequilibration, melts would have chemical signatures of successively lower pressure and more extensive melting. In this scenario, the chemical signature of melts depends critically on their ascent and segregation history.

While this somewhat speculative idea is difficult to prove, there are many independent lines of evidence suggesting that diapirs are important at slow spreading ridges. Gravity and topography data [*Lin and Phipps Morgan*, 1992; *Lin et al.*, 1990], studies of mid-ocean ridge segmentation [*Parmentier and Phipps Morgan*, 1990; *Whitehead et al.*, 1984; *Schouten et al.*, 1985; *Crane*, 1985], and theoretical studies of mantle flow [*Scott and Stevenson*, 1989; *Sotin and Parmentier*, 1989] all point to the possible importance of diapirs at slow spreading ridges. Furthermore, geologic mapping in ophiolites has

TABLE 3. Summary of Data for the 32 Best Sampled Ridges and Ridge Portions

Plot ID	Ridge	Latitude A	Longitude A	Latitude B	Longitude B	Length, km	SR, mm/yr	Range, mm/yr	CG	SD, samples / 10 km	R, $Ca_{(8)}/Al_{(8)}$	95%	R, $Na_{(8)}$	95%	Global/ Local	Quality of Match	Score
1	Mid-Cayman Rise	18.13	-81.69	18.11	-81.87	19.14	11.80	±0.00	26	13.58	0.48	+	-0.59	+	local	good	-1.13
2	Reykjanes Peninsula	63.86	-22.60	63.88	-21.50	53.88	17.58	±0.02	22	4.08	0.90	+	-0.97	+	local	good	-1.38
3	American-Antarctic Ridge	-57.71	-7.66	-56.90	-6.04	132.49	17.67	±0.21	22	1.66	0.53	+	0.14	-	local	med.	-0.24
4	North MAR (FAMOUS)	36.79	-33.27	36.92	-33.13	19.07	20.94	±0.02	113	59.26	0.39	+	-0.26	+	local	good	-1.08
5	North MAR (Narrowgate)	36.54	-33.52	36.78	-33.28	34.19	20.99	±0.04	73	21.35	0.73	+	-0.52	+	local	good	-1.56
6	North MAR (AMAR)	35.84	-34.18	36.49	-33.65	86.47	21.14	±0.10	79	9.14	0.75	+	-0.29	+	local	good	-1.30
7	North MAR (South of Kane FZ)	15.88	-46.58	23.67	-44.78	885.81	26.20	±1.21	141	1.59	0.17	+	-0.48	+	local	good	-0.54
8	Explorer Ridge (Southern segment)	48.97	-130.90	49.90	-129.50	144.61	28.00	±0.03	59	4.08	0.74	+	-0.57	+	local	good	-1.06
9	South MAR (near Triple junction)	-55.33	-1.72	-54.67	-0.02	130.83	30.70	±0.08	15	1.15	0.35	-	-0.36	-	local	poor	-0.22
10	South MAR (~26°S area)	-25.70	-13.91	-26.49	-13.76	89.05	35.67	±0.01	92	10.33	0.71	+	-0.40	+	local	good	-1.27
11	North EPR (~ 22°N area)	22.35	-108.33	23.15	-109.13	120.93	50.14	±0.42	61	5.04	0.19	-	0.07	-	local	poor	-0.06
12	North EPR (~ 20°N area)	20.82	-109.10	20.93	-109.50	43.29	52.34	±0.06	29	6.70	-0.43	+	0.67	+	global	good	1.07
13	Galapagos (90.95°-95.62°W)	2.44	-95.62	1.90	-90.95	522.02	53.98	±3.58	37	0.71	0.33	-	-0.32	-	local	poor	-0.18
14	Gorda Ridge (Northern)	42.47	-126.90	42.94	-126.60	57.69	55.00	±0.01	15	2.60	0.57	+	0.13	-	local	med.	-0.29
15	Juan de Fuca (End)	47.33	-129.00	48.20	-129.00	96.67	58.29	±0.23	46	4.76	-0.66	+	0.36	+	global	good	0.98
16	Juan de Fuca (NSR)	46.27	-129.60	47.27	-129.10	117.45	58.68	±0.15	26	2.21	0.52	+	-0.20	-	local	med.	-0.51
17	Juan de Fuca (Axial)	45.56	-130.10	46.22	-129.80	76.92	59.08	±0.25	50	6.50	-0.47	+	0.32	+	global	good	0.75
18	Juan de Fuca (B)	45.13	-130.20	45.47	-130.00	40.89	59.40	±0.07	14	3.42	-0.03	-	0.13	-	global	poor	0.11
19	Juan de Fuca (SSR)	44.53	-130.50	45.00	-130.20	57.34	59.74	±0.25	45	7.85	0.26	-	0.02	-	local	poor	-0.09
20	Galapagos (85.84°-90.81°W)	1.06	-90.81	0.76	-85.84	553.20	61.58	±3.81	42	0.76	-0.43	+	0.46	+	global	good	0.43
21	Galapagos (84.77°-85.77°W)	0.78	-85.77	1.71	-84.77	151.73	66.26	±0.77	29	1.91	-0.46	+	0.75	+	global	good	0.89
22	North EPR (13.75°-14.82°N)	13.75	-104.15	14.82	-104.39	121.67	89.92	±1.97	14	1.15	-0.30	-	0.88	+	global	med.	0.73
23	North EPR (12.91°-13.65°N)	12.91	-103.98	13.65	-104.17	84.76	93.64	±0.14	17	2.01	-0.46	-	0.93	+	global	med.	0.88
24	North EPR (12.67°-12.89°N)	12.67	-103.91	12.89	-103.97	25.30	95.48	±0.40	13	5.14	-0.90	+	0.85	+	global	good	1.36
25	North EPR (11.69°-12.57°N)	11.69	-103.81	12.57	-103.91	98.39	97.86	±1.63	95	9.66	-0.54	+	0.70	+	global	good	1.23
26	North EPR (10.29°-11.87°N)	10.29	-103.58	11.87	-103.81	177.35	101.76	±2.92	206	11.62	-0.55	+	0.51	+	global	good	1.02
27	North EPR (9.12°-10.21°N)	9.12	-104.19	10.21	-104.34	122.23	106.99	±2.02	55	4.50	-0.52	+	0.03	-	global	med.	0.61
28	North EPR (8.36°-9.12°N)	8.36	-104.14	9.12	-104.25	85.31	110.42	±1.37	30	3.52	-0.21	-	0.69	+	global	med	0.76
29	South EPR (13.08°-13.47°S)	-13.08	-110.93	-13.47	-111.10	47.08	149.60	±0.25	10	2.12	-0.09	-	0.83	+	global	med.	0.81
30	South EPR (13.22°-15.92°S)	-13.22	-112.33	-15.92	-112.98	308.06	150.89	±1.36	43	1.40	-0.15	-	0.37	+	global	med	0.32
31	South EPR (16.05°-20.52°S)	-16.05	-112.98	-20.52	-113.87	505.50	153.60	±1.26	89	1.76	-0.30	+	0.21	+	global	good	0.35
32	South EPR (21.00°-23.02°S)	-21.00	-114.19	-23.02	-114.51	226.87	155.49	±0.43	35	1.54	-0.47	+	0.64	+	global	good	0.71

Plot ID refers to the plots of Figure 5. A and B refer to the latitude and longitude of the two extreme sample localities in the segment. The length is the distance between A and B. SR is the full spreading rate at the middle point of the segment. Range is the total variation of the spreading rate of the segment. CG is the number of group means. SD is the sampling density: CG per 10 km. *R* is the correlation coefficient on the plots of $Ca_{(8)}/Al_{(8)}$ versus $Si_{(8)}/Fe_{(8)}$ and $Na_{(8)}$ versus $Si_{(8)}/Fe_{(8)}$. Plus and minus under 95% indicate either the correlation is significant or not at 95% confidence level. Global/local indicate whether the chemical systematics on both plots are of global or local trend. Quality of the match shows the "goodness of fit" of the data to either global or local trend in terms of the slopes and correlation coefficients of the regressions on the two plots. Score, determined using "goodness of fit" and sample density, is used to construct the bar chart (Figure 6). See the appendix for score procedures.

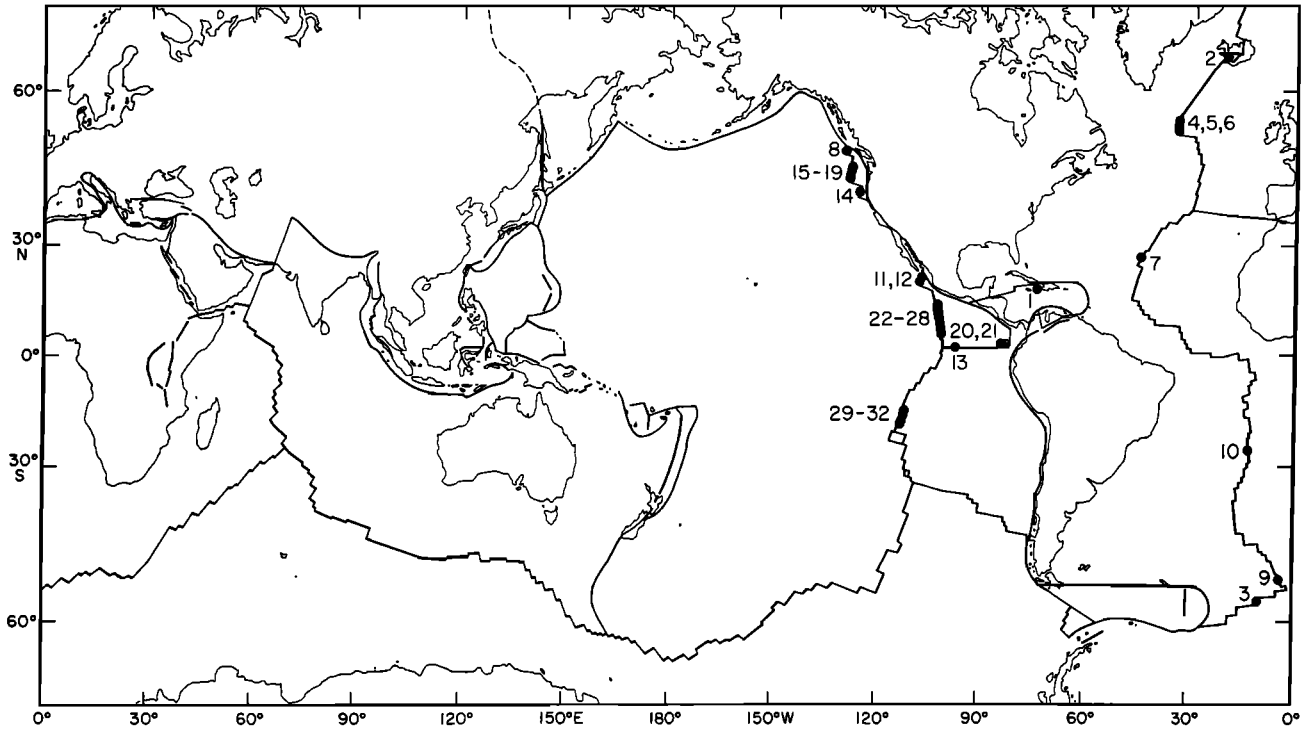

Fig. 4. Map of the mid-ocean ridge system. The 32 best sampled areas selected for this study are shown with numbers keyed to Table 3. Note the absence of well-sampled area in the Indian Ocean.

revealed diapiric structure in mantle rocks [*Rabinowicz et al.*, 1987; *Nicolas*, 1986]. These independent lines of evidence indicate that the notion of diapirs at slow spreading ridges deserves serious consideration. Assuming ascent rates of the order of plate motion rates and slow melt segregation, chemical reaction between melt and solid is difficult to avoid [*Kelemen et al.*, 1992; *Qin*, 1992]. Below, we develop this hypothesis further and offer two additional lines of supporting evidence. First, we discuss some illustrative mass balance calculations indicating that melts of the local trend could be related by a melting-crystallization reaction that plausibly could occur in rising diapirs undergoing melting and melt reequilibration. Second, we show that zero-age lavas of seamounts on the flanks of the East Pacific Rise exhibit both the global and local chemical variation trends. This is consistent with the diapir hypothesis as diapiric buoyancy instabilities may be expected to develop at the edges of the broad upwelling region below the EPR axis and flanks [*Phipps Morgan*, 1987; *Niu and Batiza*, 1991*a*]. Similarly, at transitional ridges (50–60 mm/yr) where both the global and local trends may occur, diapiric and widespread passive upwelling may both occur. In this case the petrologic signature of erupted lavas may be dominated by either trend.

Model Calculations

Relatively little is known about the physico-chemical processes occurring in mantle diapirs undergoing melting [e.g., *Ribe*, 1983; *Cawthorn*, 1975]. Under appropriate conditions, material in diapirs should melt just as passively upwelling mantle does. However, melt extraction by matrix compaction, a process thought to be generally important for upwelling mantle [*McKenzie*, 1984], could be retarded because both melt and residue rise together. In this case, the melt and matrix would have enhanced opportunity to interact chemically, even as melting continued. We envision a process similar to that studied by *Kelemen* [1990] and *Kelemen et al.* [1990] except that the process is polybaric. For this reason, the results of *Kelemen* [1990] and *Kelemen et al.* [1990] at 0.5 GPa only cannot be rigorously applied. Instead, we explore possible petrologic processes in diapirs with some extremely simple but illustrative mass balance calculations. With these calculations we attempt to directly constrain the minerals that may be involved in producing melts of the local trend of chemical variation.

A fundamental difficulty in attempting to interpret the cause of the local trend is that, by definition, this trend is composed of samples with identical MgO = 8.0 wt %. Even though the local trend probably is the result of dynamic physical and chemical processes which lead to variations in MgO (as well as other major element abundance), our present definition and view of the trend are an artificial, constant-MgO snapshot only. Whether melts forming the local trend are related to each other directly through some petrologic process such as melting or crystallization, or related only indirectly (for example, sequential products of a petrologic process), it is most improbable that they coexist as constant MgO melts.

In order to circumvent this problem of constant MgO, while at the same time trying to explicitly constrain the major silicate phases that might be involved in the local trend, we use simple stoichiometric least squares modeling of the type described by *Bryan et al.* [1969] and *Bryan* [1986]. Figure 8 shows several well-defined trends from slow spreading ridges which we use in our illustrative model. We implicitly assume that the magmas of the local trend are related to one another by some petrologic processes (melting or crystallization, for example) involving major silicate phases, and we attempt to

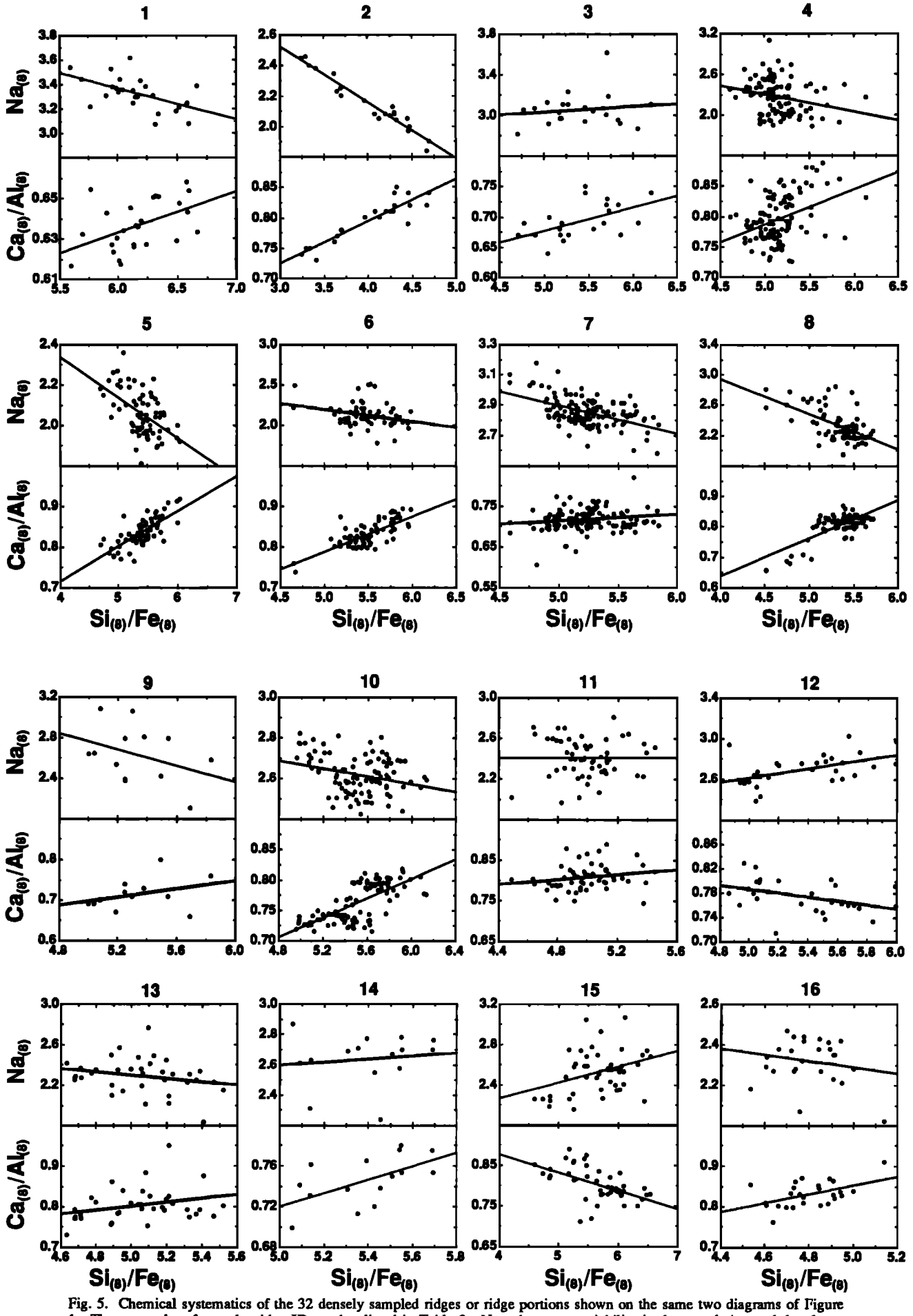

Fig. 5. Chemical systematics of the 32 densely sampled ridges or ridge portions shown on the same two diagrams of Figure 1. The numerals refer to the ridge ID number listed in Table 3. Note the great variability in the correlation and the slopes (sign and magnitude) of the regression lines. Table 3 gives correlation coefficients and values of statistical significant.

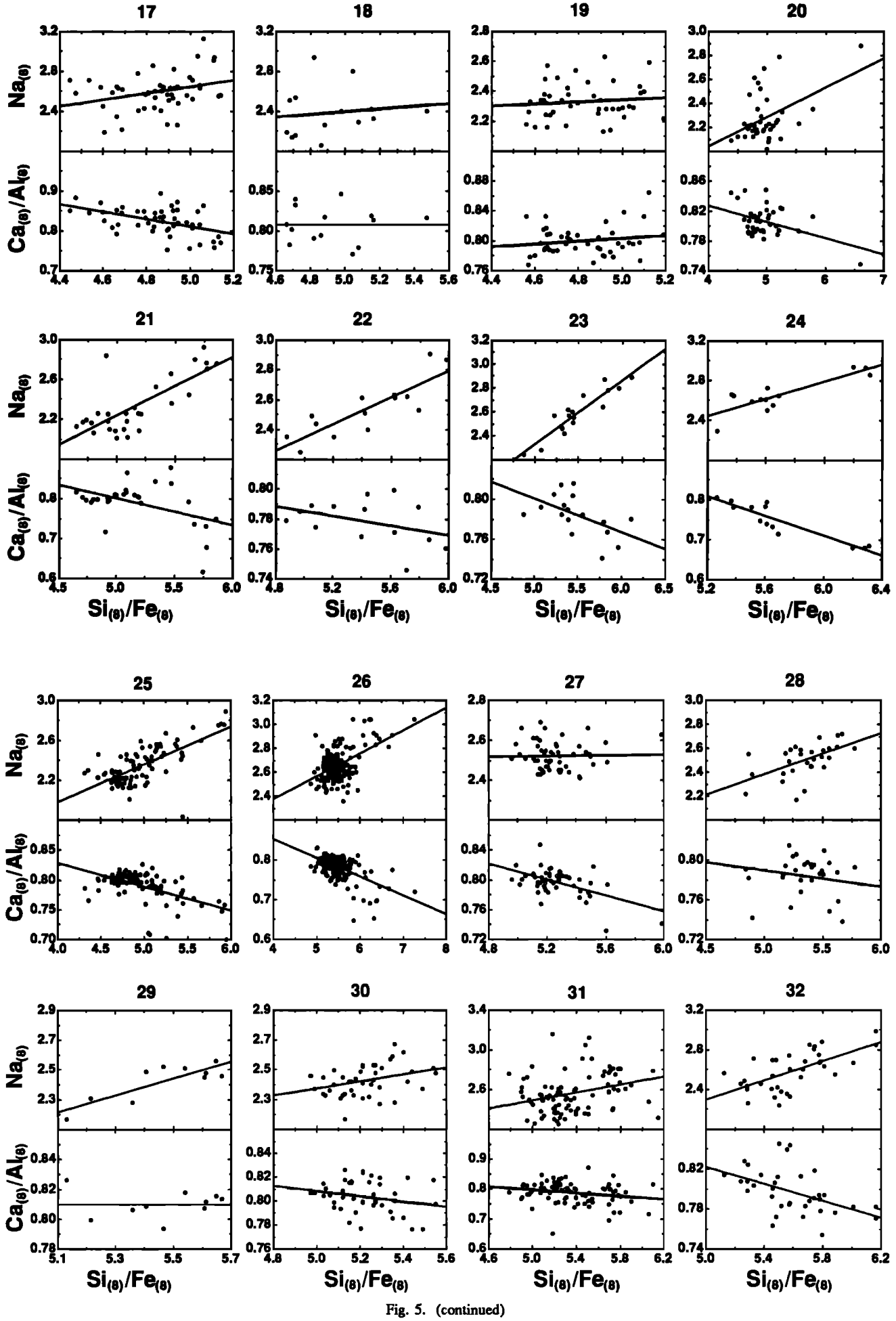

Fig. 5. (continued)

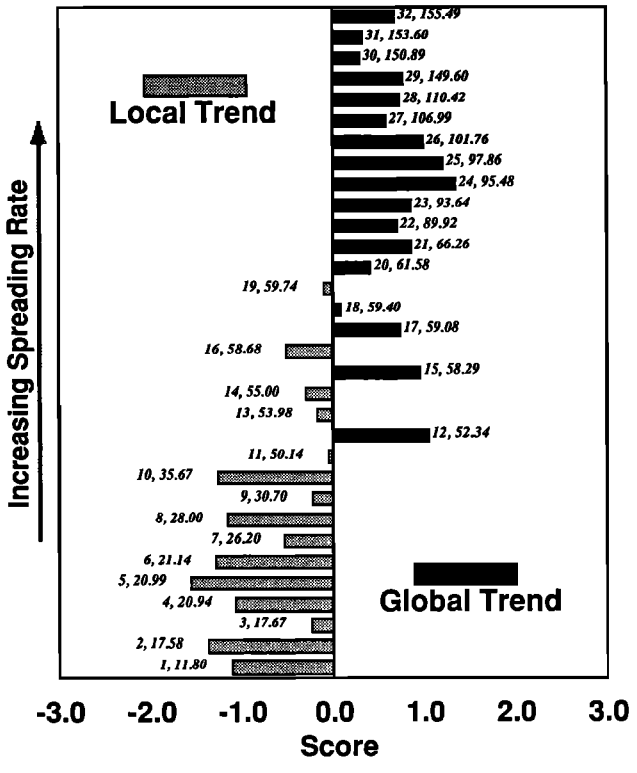

Fig. 6. Bar diagrams to show the relationships between chemical systematics and the full spreading rate. Each bar refers to a specific ridge segment listed in Table 3 and the first number gives its ID number. The value after the comma is the full spreading rate. This figure clearly shows that fast spreading ridges exhibit the global trend and slow spreading ridges the local trend. There is also a transition (50–60 mm/yr) where either trend is possible.

determine the phases and their proportions using mole percent least squares mass balance calculations.

For simplicity, in Figure 9 we omit data points and show only the regression lines for each of the local trends. We essentially ask what assemblages of silicate phases could be involved in producing the trend from *a* to *b* (or *b* to *a*)? To get around the problem of constant MgO, we use a two step approach. First, in the stoichiometric modeling, we combine Fe and Mg to form one divalent cation (FM). This allows us to obtain a first-order solution while, for the moment, neglecting the constant MgO problem. Using FM also allows us to temporarily disregard the complexity of Fe/Mg partitioning in natural silicate phases and the effects of pressure, temperature and composition on the partitioning behavior as we seek only a generalized solution. But having done the initial modeling with FM, we return to consider how much MgO may actually change along the *a*–*b* or *b*–*a* paths of Figure 9.

With the cation FM, we make olivine (FM_2SiO_4) and pyroxene ($FM_2Si_2O_6$: both orthopyroxene and Mg-Fe components of clinopyroxene). In this simple stoichiometric modeling, we also consider endmember diopside-hedenbergite, jadeite, Ca-tschermaks, and albite-anorthite. Table 4 shows the liquid compositions at points *a* and *b* of each of the local trends of Figures 8 and 9. We then use a least-squares method to determine the stoichiometric endmember phases which can, when added to liquid *a*, produce liquid *b* (or vice versa).

While least-squares mixing models of this type, especially with few components and many phases, are notorious for giving non-unique solutions, our result appear to be very robust. We have tested hundreds of models using many combinations of mineral end members but only a few yield self-consistent results with good fits (low residuals). Representative results are shown in Table 5. Note that the poorest fits are for Ti and K, which is not surprising since we did not include mineral endmembers containing either element (though we could add Ti to pyroxene). One interesting result is that plagioclase is apparently not needed to describe the *a*–*b* path for any locality as all solutions with plagioclase give very high residuals (> 2.0 or so), with especially poor fits for Ca and Al. This is not surprising because melting in plagioclase stability field may be quite restricted [*Nicolas*, 1986]. Table 5 shows that in general, the path from *a* to *b* (Figure 9) seems to involve both melting and crystallization. Pyroxene components are taken into liquid *a* while olivine solidifies; together, these two effects produce liquid *b*. In all four cases, the original liquid *a* represents about half of the eventual liquid *b*, and the ratio of pyroxene components (added to melt) to olivine component (removed from the melt) is 3.6–4.0. Such a trend is thus a net melting trend characterized by a mineral–melt reaction of the general form:

$$\text{liquid } a + \text{pyroxene} \Leftrightarrow \text{liquid } b + \text{olivine}$$

and is similar to the reactions studied theoretically and experimentally by *Kelemen* [1990] and *Kelemen et al.* [1990] at 0.5 GPa. Under conditions of ascent to lower pressure, this reaction would proceed to the right [e.g., *O'Hara*, 1965; *Stolper*, 1980; and *Elthon and Scarfe*, 1984], obviously favoring the *a* to *b* path over the alternative *b* to *a* path.

This result seems reasonable and is consistent with processes expected in a buoyant solid-liquid diapir undergoing

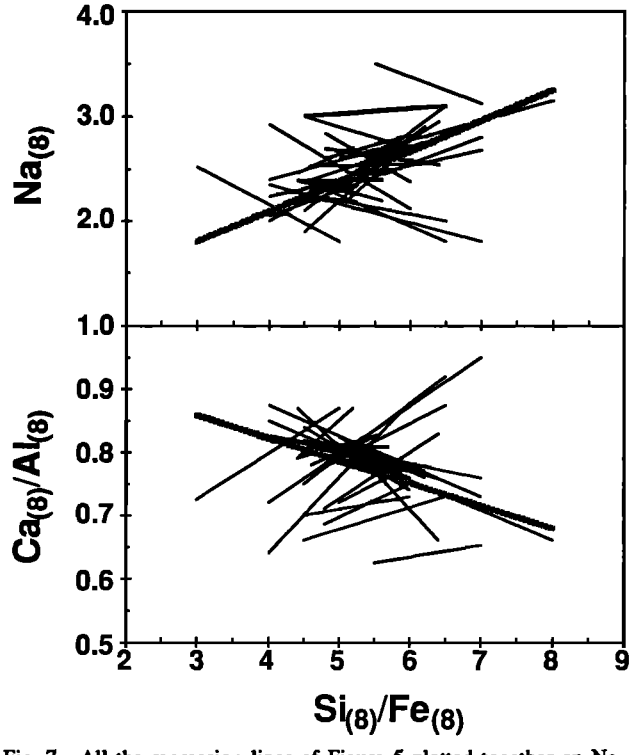

Fig. 7. All the regression lines of Figure 5 plotted together on $Na_{(8)}$ and $Ca_{(8)}/Al_{(8)}$ versus $Si_{(8)}/Fe_{(8)}$ diagrams. The heavy line (for reference) is the global trend from Figure 4. Note that the slopes of both the local and global trends vary and that no simple pattern (such as a fanning pattern) exists.

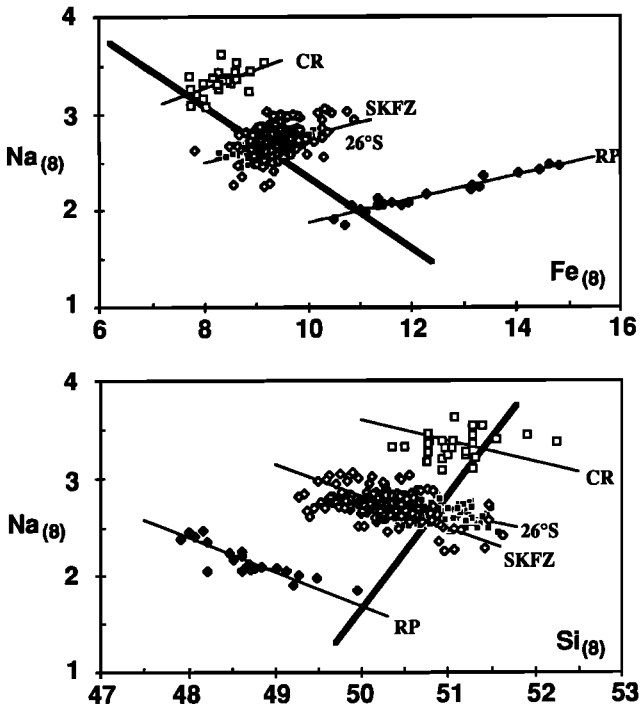

Fig. 8. Plots of $Na_{(8)}$ versus $Fe_{(8)}$ and $Na_{(8)}$ versus $Si_{(8)}$ showing the global trend of *Klein and Langmuir* [1989] (thick line) and several best defined local trends (cross trends) recognized at slow spreading mid-ocean ridge segments [*Klein and Langmuir*, 1989; *Batiza et al.*, 1988]. CR, Cayman Rise; 26°S, MAR at 26°S; SKFZ, MAR south of the Kane Fracture Zone; and RP, Reykjanes Peninsula.

additional melting. Note that in Table 5 the combined compositions of the pyroxenes entering the melts are unlike any natural pyroxenes in that Jd, and particularly Ct, are too high. This is, in fact, expected, as both orthopyroxene and clinopyroxene are residual phases during mantle melting to produce MORB [*Dick et al.*, 1984]. Continuous melting will tend to deplete Jd and Ct components in residual pyroxenes because both are incompatible during melting and less stable in pyroxenes as pressure is reduced. Thus pyroxenes in the solid will gradually be depleted in these components, while the melt in a rising diapir will be enriched in Jd and Ct components.

We now reconsider possible changes in MgO and FeO. To calculate the MgO and FeO changes, we dispense with the use of FM. Using the phase proportions from Table 5, we partition FeO and MgO among the solid silicate phases (see Table 4 note for details) and calculate liquid *b* as a combination of liquid *a* and the phases of Table 5. The FeO and MgO values obtained are given in Table 4. MgO changes only slightly along our calculated path *a* – *b*. It is important to note that because of the MgO = 8.0 condition of the local trend lines in Figures 8 and 9 and because the calculations indicate a small change of MgO, the calculated *a* – *b* paths cannot be identical to the *a* – *b* paths of the local trends. To assess the difference in the calculated versus observed paths, we plot the calculated endpoints (*b*) on Figure 9. In addition, we plot local trends corrected to MgO = 7.0 and MgO = 9.0, which fall close to the MgO = 8.0 positions. Thus, while the calculated *a* – *b* paths are not identical to the slow spreading data arrays in Figure 9, they are very close. Indeed, since the slopes of actual local trends vary (Figure 7), there is evidently some variability in the processes leading to this trend. Given the potential complexity of physical-chemical processes in rising diapirs undergoing melting, this variability in the data is not surprising.

Kinzler and Grove [1992] recently proposed polybaric fractional crystallization as a possible origin for the local trend. We feel that fractional crystallization is inevitable within rising mantle diapirs, but such fractionation should occur only during the latest stages of diapirism when melting ceases due to slow ascent and higher heat loss. Mineralogic features of MORB lavas from slow spreading ridges suggest that polybaric fractionation may play a role in their petrogenesis [*Bryan et al.*, 1981; *Juster et al.*, 1989]. However, we suggest that polybaric fractionation should not be the major cause of the local trend; a rigorous model should explain the chemical relationships among parameters of Fe, Si, Ca, Al, and Na as shown above, not just Fe and Si versus Na. A rigorous test among existing models requires much additional study of possible processes in diapirs, plus careful petrologic modeling of both melting residue (peridotite) and individual lava suites that exhibit the local trend.

Evidence From Near-EPR Seamounts

The near-axis flanks of the EPR have abundant seamounts composed dominantly of MORB [*Batiza et al.*, 1990]. They occur as individual seamounts and also as chains parallel to either relative or absolute plate motion. Figure 10 shows that the seamount array is very similar to the global array (defined using axial samples only) (Figure 1) and appears to be a

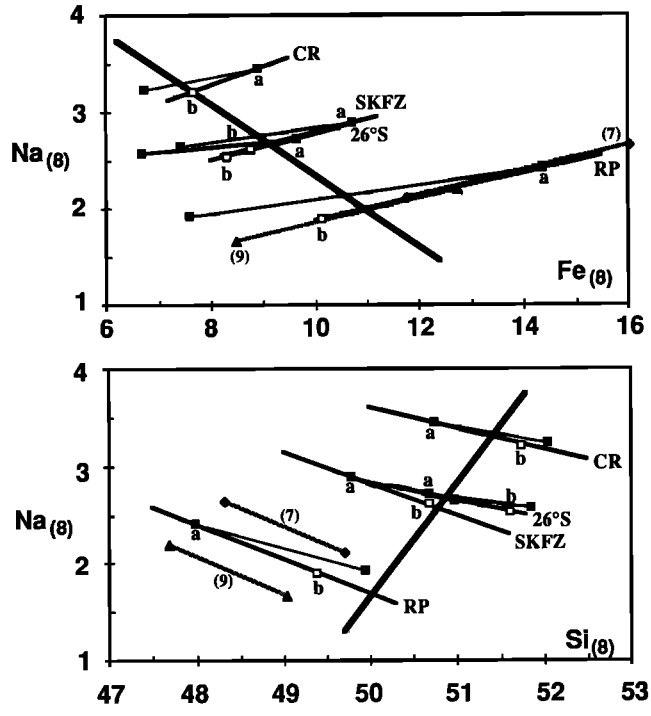

Fig. 9. Same as Figure 8 but with the data points of the local trends omitted. Regression lines are best fit lines for all elements (not just ones shown). The points labeled *a* (solid square) and *b* (empty square) are the liquids we consider in Tables 4 and 5 which define the *a*–*b* path we attempt to model. The thin lines between solid squares are the results of our two-step modeling procedure (see Tables 4 and 5 and text for details). Note that the thin lines (model) and the thick lines (data) are generally well matched. The model we present gives a good fit to all elements, not just Na, Fe, and Si. Also shown as thin light lines for comparison are the local trend data corrected to MgO = 7.0 and 9.0 wt % as labeled (RP only, others are similar). Note that these data have similar slopes to the MgO = 8.0 wt % local trend.

TABLE 4. Melt Compositions for Each Local Trend (Figures 8 and 9)

	RP–*a*	RP–*b*	CR–*a*	CR–*b*	SK–*a*	SK–*b*	26°S–*a*	26°S–*b*
				Weight Percent at MgO = 8%				
$Si_{(8)}$	48.00	49.38	50.75	51.75	49.80	50.69	50.69	51.62
$Ti_{(8)}$	2.48	1.06	1.67	1.46	1.85	1.28	1.68	1.13
$Al_{(8)}$	13.56	15.60	16.14	16.79	15.30	16.25	15.48	15.70
$Fe_{(8)}$	14.37	10.13	8.91	7.68	10.73	8.78	9.65	8.31
$Ca_{(8)}$	10.12	13.15	10.11	10.85	10.55	11.88	11.48	12.41
$Na_{(8)}$	2.41	1.89	3.45	3.20	2.89	2.61	2.70	2.52
$K_{(8)}$	0.25	0.10	0.23	0.28	0.23	0.20	0.09	0.06
$P_{(8)}$	0.24	0.07	0.18	0.18	0.19	0.13	0.16	0.11
MgO*		9.55		8.74		8.76		9.58
FeO*		8.01		6.71		7.38		6.59
				Recalculated to Cation Mole Percent				
Si	45.35	46.19	46.82	47.32	46.33	46.82	46.93	47.69
Ti	1.77	0.75	1.16	1.00	1.30	0.89	1.17	0.78
Al	15.10	17.19	17.55	18.10	16.77	17.70	16.90	17.09
FM†	22.63	19.08	17.88	16.78	19.44	17.80	18.52	17.44
Ca	10.25	13.18	10.00	10.63	10.52	11.76	11.39	12.29
Na	4.42	3.44	6.19	5.70	5.22	4.69	4.87	4.54
K	0.30	0.12	0.27	0.33	0.27	0.23	0.11	0.07
P	0.19	0.06	0.14	0.14	0.15	0.11	0.12	0.09

RP, Reykjanes Peninsula; CR, Cayman Rise; SK, south of The Kane Fracture Zone; and 26°S, 26°S area MAR.

*MgO and FeO compositions for *b* were calculated explicitly to determine their change along the *a*–*b* path. In this calculation, other elements agree with those in Table 5. We used the calculated phase proportions from Table 5 and peridotite modal abundances from *Dick* [1989]. We partition En-Fs between Opx and Cpx in Table 5 in the ratio 63:37, with Opx free of Di and Hd components. We also used $Fo_{90.3}$, Opx with $Mg^{\#} = 91.3$ and Cpx with $Mg^{\#} = 94.6$ from *Dick* [1989]. As explained in the text, we consider these mass balance models illustrative, not definitive.

† FM is the combined cation mole percent of FeO and MgO (= 8.0 wt %).

TABLE 5. Results of the Least Squares Model Calculations

	RP–*b*	CR–*b*	SK–*b*	26°S–*b*
a	0.4884	0.6816	0.6667	0.5414
Di-Hd	0.1569	0.0599	0.0841	0.1249
Jd	0.0518	0.0597	0.0488	0.0767
Ct	0.1704	0.0929	0.1060	0.1204
En-Fs	0.2913	0.2220	0.2104	0.2816
Ol	-0.1569	-0.1200	-0.1167	-0.1467
SQ'D	0.0142	0.0654	0.0032	0.0220

	RP–*b*			CR–*b*			SK–*b*			26°S–*b*		
	Calc	Obser	Diff	Calc	Obser	Diff	Calc	Obser	Diff	Calc	Obser	Diff
Si	46.18	46.19	-0.01	47.32	47.32	0.00	46.82	46.82	0.00	47.68	47.69	-0.01
Ti	0.86	0.75	0.11	0.79	1.00	-0.21	0.87	0.89	-0.02	0.63	0.78	-0.15
Al	17.19	17.19	0.00	18.10	18.10	0.00	17.70	17.70	0.00	17.09	17.09	0.00
FM	19.08	19.08	0.00	16.78	16.78	0.00	17.80	17.80	0.00	17.44	17.44	0.00
Ca	13.19	13.18	0.01	10.64	10.63	0.01	11.77	11.76	0.01	12.30	12.29	0.01
Na	3.45	3.44	0.01	5.71	5.70	0.01	4.70	4.69	0.01	4.55	4.54	0.01
K	0.15	0.12	0.03	0.18	0.33	-0.15	0.18	0.23	-0.05	0.06	0.07	-0.01

Di-Hd, diopside-hedenbergite; Jd, jadeite; Ct, Ca-tschermaks; En-Fs, enstatite-ferrosilite; Ol, olivine; SQ'D, sum of residuals squared (Σr^2). Calc, calculated; Obser, observed; and Diff, difference. All the elements are cation mole percent.

combination of both the global and local trends. Very clear local trends are found at individual seamounts, as shown in Figure 11. Thus the local trend is not confined to slow spreading ridges but also is found from zero-age lavas of seamounts near fast spreading ridges.

As shown by *Niu and Batiza* [1991*a*], mantle upwelling beneath the EPR appears to become less vigorous off axis such that at 40–50 km away from the EPR axis the upwelling is feeble. In such an off-axis mantle setting, diapiric instabilities would have adequate time to nucleate and rise, providing MORB melts for some off-axis active volcanoes. While this suggestion is speculative, the existence of diapiric

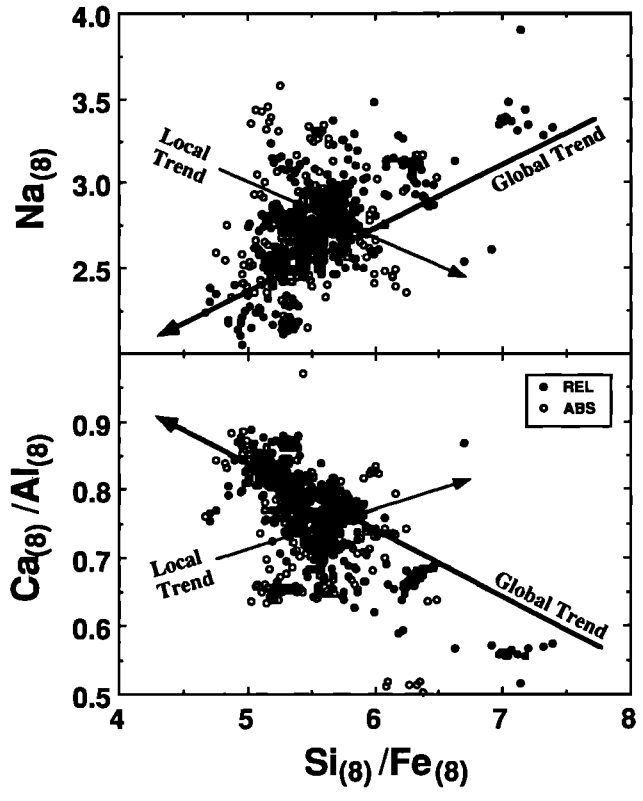

Fig. 10. Data for seamounts near East Pacific Rise (8° to 15°N) from *Batiza and Vanko* [1984], *Allan et al.* [1989], *Batiza et al.* [1989, 1990], and unpublished data. REL points are from members of small seamount chains parallel to relative motion; ABS for chains parallel to the absolute plate motion. For reference, we show the global trend [*Klein and Langmuir*, 1989], a representative local trend and data for the northern EPR from *Niu and Batiza* [1991*a*]. Note that the seamount data array strongly resembles the global axial MORB array (Figure 1).

instabilities below the flanks of the EPR is very plausible. If so, then the existence of the local trend at near-EPR seamounts is consistent with the other lines of evidence indicating that the local trend could originate by solid-melt reaction in rising diapirs undergoing melting.

Diapirs at Slow Spreading Ridges

Slow spreading ridge segments in the Atlantic [e.g., *Kuo and Forsyth*, 1991; *Lin et al.*, 1990] are typically characterized by central along-axis highs and negative residual gravity anomalies. These anomalies may be due to thick crust, a thicker mantle column of low-density residual mantle, and/or higher-temperature mantle. All these possibilities are consistent with focused buoyant mantle upwelling with more melting in the center of the segment. Whether this represents a single large diapir or numerous individual diapirs in the center of the segment is not known. Nevertheless, given the numerous independent lines of evidence favoring diapirs at slow spreading ridges, plus the two additional petrological lines of evidence presented above, we suggest a diapir model for the origin of the local trend of chemical variation.

CONCLUSIONS

1. With an expanded global data set, we confirm that slow spreading ridges generally appear to have more primitive lavas than fast spreading ridges.

2. We confirm that there appear to be no systematic differences between slow and fast spreading ridges in the depth or extent of partial melting; thus mantle temperature seems to be independent of spreading rate.

3. The so-called local and global trends of MORB systematics are a function of spreading rate. The global systematics are found at fast spreading ridge segments and the local systematics are found at slow spreading ridges. Either trend can be found in transitional ridges spreading at 50–60 mm/yr.

4. The so-called local and global trends are not apparently sensitive to geographic length scale.

5. The global and local trends display a range of slopes on chemical diagrams, but no consistent or regular behavior, such as a fanning pattern.

6. The local trend is not confined to slow spreading ridges but also occurs at near-EPR seamounts.

7. Strong geophysical and field evidence (in ophiolites) points to the importance of diapirs at slow spreading ridges. We show that the local trend is characteristic of slow spreading ridges and propose that this trend could result from processes in rising diapirs undergoing melting and melt reequilibration.

8. Transitional ridges spreading at 50–60 mm/yr may display either the global or local trend of chemical variation. We interpret this to indicate that both two-dimensional, passive upwelling and buoyant, three-dimensional (diapiric) mantle upwelling occur and that the petrologic signatures of lavas erupted may be dominated by either process.

APPENDIX

Numerical values (scores) are derived to objectively assess how well the observed trends match idealized local and/or global trend.

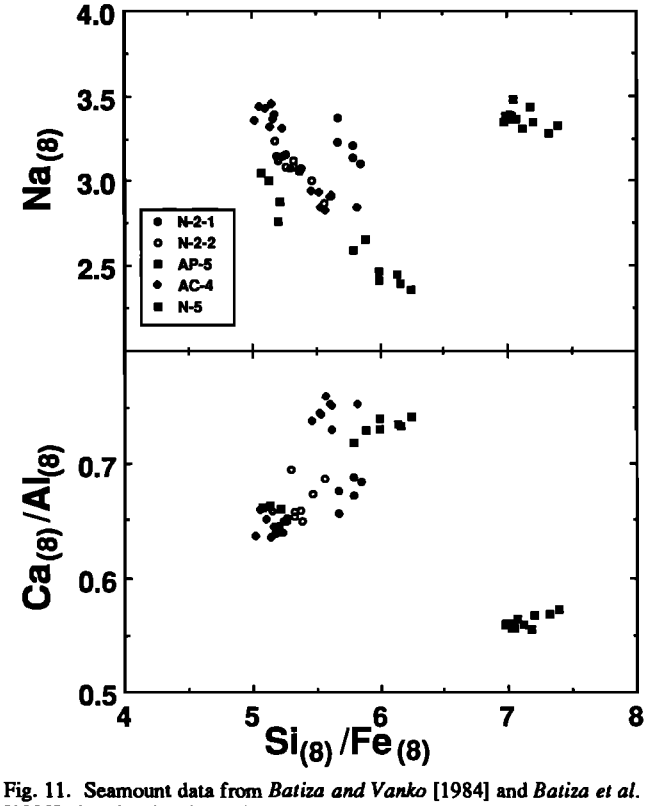

Fig. 11. Seamount data from *Batiza and Vanko* [1984] and *Batiza et al.* [1990] showing local trends for individual seamounts.

$R_{Ca/Al}$ and R_{Na} are the correlation coefficients of $Ca_{(8)}/Al_{(8)}$ versus $Si_{(8)}/Fe_{(8)}$ and $Na_{(8)}$ versus $Si_{(8)}/Fe_{(8)}$, respectively; $R^{95\%}$ is the critical value of the correlation coefficient at 95% confidence level (t test); In our test, if the R is significant at 95% confidence level, the slopes of the regression lines are also significant at that level (F test).

Local trend

Good (-1.0): $R_{Ca/Al} > 0$, $R_{Na} < 0$, $R_{Ca/Al}$ and $|R_{Na}| > R^{95\%}$
Med (-0.8): $R_{Ca/Al} > 0$, $R_{Na} < 0$, $R_{Ca/Al}$ or $|R_{Na}| > R^{95\%}$
Poor (-0.6): $R_{Ca/Al} > 0$, $R_{Na} < 0$, $R_{Ca/Al}$ and $|R_{Na}| \le R^{95\%}$

Global trend

Good (1.0): $R_{Ca/Al} < 0$, $R_{Na} > 0$, $|R_{Ca/Al}|$ and $R_{Na} > R^{95\%}$
Med (0.8): $R_{Ca/Al} < 0$, $R_{Na} > 0$, $|R_{Ca/Al}|$ or $R_{Na} > R^{95\%}$
Poor (0.6): $R_{Ca/Al} < 0$, $R_{Na} > 0$, $|R_{Ca/Al}|$ and $R_{Na} \le R^{95\%}$,

Transitional

Local med (-0.4): $R_{Ca/Al} > 0$, $R_{Na} \ge 0$, Larger $R > R^{95\%}$
or $R_{Ca/Al} \le 0$, $R_{Na} < 0$, $|\text{Larger } R| > R^{95\%}$
Local poor (-0.2): $R_{Ca/Al} > 0$, $R_{Na} \ge 0$, Larger $R \le R^{95\%}$
or $R_{Ca/Al} \le 0$, $R_{Na} < 0$, $|\text{Larger } R| \le R^{95\%}$
Global med (0.4): $R_{Ca/Al} < 0$, $R_{Na} \le 0$, $|\text{Larger } R| > R^{95\%}$
or $R_{Ca/Al} \ge 0$, $R_{Na} > 0$, Larger $R > R^{95\%}$
Global poor (0.2): $R_{Ca/Al} < 0$, $R_{Na} \le 0$, $|\text{Larger } R| \le R^{95\%}$
or $R_{Ca/Al} \ge 0$, $R_{Na} > 0$, Larger $R \le R^{95\%}$

Calculated score for plotting is to reflect the important effects of the R values and the sampling density along a ridge segment, we calculated the plotted scores by

$$\text{Score} = \text{AGF} * R * \text{SD}^{1/4}$$

where AGF is the arbitrary "goodness of fit" (values in parentheses after Good, Med, and Poor); R is the larger correlation coefficient; and SD is the sample density (number of chemical group means per 10 km). We arbitrarily use the radical of 4 to damp out the large range of values for sampling density while arbitrarily keeping our score numerically small.

Acknowledgments. We thank R. Hey and J. Karsten for help at various stages of the work and J. Sinton for discussions. We also thank J. Allan, J. Brophy, R. Hekinian, W. Bach, and K. Harpp for very helpful comments on an early version of the paper. E. Klein, P. Michael, and J. Lin provide very helpful reviews. This work was supported by NSF (OCE-89-96191, and OCE-90-00193) and the Office of Naval Research. The final revision is supported by a L-DEO Postdoctoral Fellowship to YN. This is SOEST contribution 3079.

REFERENCES

Allan, J. F., R. Batiza, M. R. Perfit, D. J. Fornari, and R. O. Sack, Petrology of lavas from the Lamont seamount chain and adjacent East Pacific Rise, 10°N, *J. Petrol., 30*, 1245-1298, 1989.

Anderson, R. N., D. A. Clague, K. D. Klitgord, M. Marshall, and R. K. Nishimori, Magnetic and petrologic variations along the Galapagos spreading center and their relation to the Galapagos melting anomaly, *Geol. Soc. Am. Bull., 86*, 683-694, 1975.

Anderson, R. N., D. J. Sparious, J. K. Weissel, and D. E. Hayes, The interrelation between variations in magnetic anomaly amplitudes and basaltic magnetization and chemistry along the Southeast Indian ridge, *J. Geophys. Res., 85*, 3883-3898,1980.

Batiza, R., Inverse relationship between Sr isotope diversity and rate of oceanic volcanism has implications for mantle heterogeneity, *Nature, 309*, 440-441, 1984.

Batiza, R., The Pacific Ocean Basin, in *Oceanic Basalts*, edited by P. A. Floyd, pp. 246-288, Blackie Glasgow, 1991.

Batiza, R. and Y. Niu, Petrology and magma chamber processes at the East Pacific Rise ~ 9°30'N, *J. Geophys. Res., 97*, 6779-6797, 1992.

Batiza, R. and D. A. Vanko, Petrology of young Pacific seamounts, *J. Geophys. Res., 89*, 11,235-11,260, 1984.

Batiza, R., W. G. Melson, and T. O'Hearn, Simple magma supply geometry inferred beneath a segment of the Mid-Atlantic Ridge, *Nature, 335*, 428-431, 1988.

Batiza, R., T. L. Smith, and Y. Niu, Geologic and Petrologic evolution of seamounts near the EPR based on submersible and camera study, *Mar. Geophys. Res., 11*, 169-236, 1989.

Batiza, R, Y. Niu, and W. C. Zayac, Chemistry of seamounts near the East-Pacific Rise: Implications for the geometry of sub-axial mantle flow, *Geology, 18*, 1122-1125, 1990.

Bender, J. F., C. H. Langmuir, and G. N. Hanson, Petrogenesis of basalt glasses from the Tamayo region, East Pacific Rise, *J. Petrol., 25*, 213-254, 1984.

Blackman, D. K., and D. W. Forsyth, Gravity and tectonics on the Mid-Atlantic Ridge 25° -27°30'S, *J. Geophys. Res., 96*, 11,741-11,758, 1991.

Botros, M., and H. P. Johnson, Tectonic evolution of the Explorer-northern Juan de Fuca region from 8 Ma to the present, *J. Geophys. Res., 93*, 10,421-10,437, 1988.

Bougault, H., and R. Hekinian, Rift valley in the Atlantic Ocean near 36°50'N: Petrology and geochemistry of basaltic rocks, *Earth Planet. Sci. Lett., 24*, 249-261, 1974.

Bougault, H., L. Dmitriev, J.-G. Schilling, A. Sobolev, J. L. Jordan, and H. D. Needham, Mantle heterogeneity from trace elements: MAR triple junction near 14°N, *Earth Planet. Sci. Lett., 88*, 27-36, 1988.

Brodholt, J. P., and R. Batiza, Global systematics of unaveraged mid-ocean ridge basalt compositions: Comments on "Global correlations of ocean ridge basalt chemistry with axial depth and crustal thickness by E. M. Klein and C. H. Langmuir", *J. Geophys. Res., 94*, 4231-4239, 1989.

Bryan, W. B., Regional variation and petrogenesis of basalt glasses from the FAMOUS area, Mid-Atlantic Ridge, *J. Petrol., 20*, 293-325, 1979.

Bryan, W. B., Linked evolutionary data arrays: A logical structure for petrologic modeling of multisource, multiprocess magmatic systems, *J. Geophys. Res., 91*, 5891-5900, 1986.

Bryan, W. B., and J. G. Moore, Compositional variations of young basalts in the Mid-Atlantic Ridge rift valley near lat. 36°49'N, *Geol. Soc. Am. Bull., 88*, 556-570, 1977.

Bryan, W. B., L. W. Finger, and F. Chayes, Estimating proportions in petrological mixing equations by least-squares approximation. *Science, 163*, 926-927, 1969.

Bryan, W. B., G. Thompson, and J. N. Ludden, Compositional variations in normal mid-ocean ridge basalt from 22°–25°N: Mid-Atlantic Ridge and Kane Fracture Zone, *J. Geophys. Res., 86*, 11,815–11,836, 1981.

Byers, C. D., M. O. Garcia, and D. W. Muenow, Volatiles in basaltic glasses from the East Pacific Rise at 21°N: Implications for MORB sources and submarine lava flow morphology, *Earth Planet. Sci. Lett., 79*, 9-20, 1986.

Campsie, J., G. L. Johnson, M. H. Rasmussen, and J. Laursen, Dredged basalts from the western Nazca plate and the evolution of the East Pacific Rise, *Earth Planet. Sci. Lett., 68*, 271-285, 1984.

Cawthorn, R. G., Degrees of melting in mantle diapirs and the origin of ultramafic liquids, *Earth Planet. Sci. Lett., 27*, 113-120, 1975.

Christie, D. M., and J. M. Sinton, Major element constraints on melting, differentiation and mixing of magmas from the Galapagos 95.5°W propagating rift system, *Contrib. Mineral. Petrol., 94*, 274-288, 1986.

Clague, D. A., F. A. Frey, G. Thompson, and S. Rindge, Minor and trace element geochemistry of volcanic rocks dredged from the Galapagos spreading center: Role of crystal fractionation and mantle heterogeneity, *J. Geophys. Res., 86*, 9469-9482, 1981.

Cohen, R. S., and R. K. O'Nions, The lead, neodymium and strontium isotopic structure of ocean ridge basalts, *J. Petrol., 23*, 299-324, 1982.

Cousens, B. L., R. L. Chase, and J.- G. Schilling, Basalt geochemistry of Explorer area, northeast Pacific Ocean, *Can. J. Earth Sci., 21*, 157-170, 1984.

Crane, K., The spacing of rift axis highs: Dependance on diapiric processes in the underlying asthenosphere?, *Earth Planet. Sci. Lett.*, *72*, 405–415, 1985.

Davis, A. S., and D. A. Clague, Geochemistry, mineralogy and petrogenesis of basalt from the Gorda Ridge, *J. Geophys. Res.*, *92*, 10,467-10,483, 1987.

DeMets, C, R. G. Gordon, D.F. Argus, and S. Stein, Current plate motions, *Geophys. J. Int.*, *101*, 425-478, 1990.

Dick, H. J. B., Abyssal peridotites, very slow spreading ridges and ocean ridge magmatism, in Magmatism in Ocean Basins, edited by A. D. Saunders and M. J. Norry, *Gel. Soc. Spec. Publ. London*, *42*, 71-106, 1989.

Dick, H. J. B., R. L. Fisher, and W. B. Bryan, Mineralogical variability of the uppermost mantle along mid-ocean ridges, *Earth Planet. Sci. Lett.*, *69*, 88–106, 1984.

Dickey, J. S., Jr., F. A. Frey, S. R. Hart, E. B. Watson, and G. Thompson, Geochemistry and petrology of dredged basalts from the Bouvet triple junction, South Atlantic, *Geochim. Cosmochim. Acta*, *41*, 1105-1118, 1977.

Dosso, L., H. Bougault, P. Beuzart, J.-Y. Calvez, and J.-L. Jordan, The geochemical structure of the South-East Indian ridge, *Earth Planet. Sci. Lett.*, *88*, 47-59, 1988.

Eaby, J., D. A. Clague, and J. R. Delaney, Sr isotopic variations along the Juan de Fuca ridge, *J. Geophys. Res.*, *89*, 7883-7890, 1984.

Elthon, D., and C. M. Scarfe, High-pressure phase equilibria of a high-magnesian basalt and the genesis of primary oceanic basalts, *Am. Mineral.*, *69*, 1-15, 1984.

Engel, C. G., and R. L. Fisher, Granitic to ultramafic rock complex of the Indian Ocean ridge system, western Indian Ocean, *Geol. Soc. Am. Bull.*, *86*, 1553-1578, 1975.

Fisk, M. R., A. E. Bence, and J.- G. Schilling, Major element chemistry of Galapagos rift zone magmas and their phenocrysts, *Earth Planet. Sci. Lett.*, *61*, 171-189, 1982.

Flower, M. J. F., Thermal and kinematic control on ocean-ridge magma fractionation: Contrasts between Atlantic and Pacific spreading axes, *J. Geol. Soc. London*, *138*, 695-712, 1980.

Franchteau, J., and R. D. Ballard, The East Pacific Rise near 21°N, 13°, and 20°S: inferences from along-strike variability of axial processes of the mid-ocean ridges, *Earth Planet. Sci. Lett.*, *64*, 93-116, 1983.

Hamelin, B., and C. J. Allègre, Large scale regional units in the depleted upper mantle: Revealed by an isotopic study of the Southwest Indian Ridge, *Nature*, *315*, 196-199, 1985.

Hawkins, J. W., and J. T. Melchior, Descriptive catalogue of basalt samples from the East Pacific Rise at 21°N, *SIO Ref. 80-4*, Scripps Inst. of Oceanogr., Univ. of Calif., San Diego, 1980.

Hayes, D. E., and A. K. Kane, The dependence of seafloor roughness on spreading rate, *Geophys. Res. Lett.*, *18*, 1425-1428, 1991.

Hekinian, R., and D. Walker, Diversity and spatial zonation of volcanic rocks from the East Pacific Rise near 21°N, *Contrib. Mineral. Petrol.*, *96*, 265-280, 1987.

Hekinian, R., J. M. Auzende, J. Francheteau, P. Gente, W. B. F. Ryan, and E. S. Kappel, Offset spreading centers near 12°53'N on the East Pacific Rise: Submersible observations and composition of the volcanics, *Mar. Geophys. Res.*, *7*, 359-377, 1985.

Hekinian, R., G. Thompson, and D. Bideau, Axial and off-axial heterogeneity of basaltic rocks from the East Pacific Rise at 12°35'N–12°51'N, *J. Geophys. Res*, *94*, 17,437-17,463, 1989.

Holness, M. B., and F. M. Richter, Possible effects of spreading rate on MORB isotopic and rare earth composition arising from melting of a heterogeneous source, *J. Geol.*, *97*, 247-260, 1989.

Humler, E., and H. Whitechurch, Petrology of basalts from the Central Indian ridge (lat. 25°23'S, long. 70°04'E): Estimates of frequencies and fractional volumes of magma injections in a two-layered reservoir, *Earth Planet. Sci. Lett.*, *88*, 169-181, 1988.

Humphris, S. E., G. Thompson, J.-G. Schilling, and R. H. Kingsley, Petrological and geochemical variations along the Mid-Atlantic Ridge between 46°S and 32°S: Influence of the Tristan de Cunha mantle plume, *Geochim. Cosmochim. Acta*, *49*, 1445-1464, 1985.

Ito, E., W. M. White, and C. Göpel, The O, Sr, Nd, Pb isotope geochemistry of MORB, *Chem. Geol.*, *62*, 157-176, 1987.

Jaköbsson, S. P., J. Jónsson, and F. Shido, Petrology of the western Reykjanes Peninsula, Iceland, *J. Petrol.*, *19*, 669-705, 1978.

Juster, T. C., T. L. Grove, and M. R. Perfit, Experimental constraints on the generation of FeTi basalts, andesites, and rhyodacites at the Galapagos spreading center, 85°W and 95°W, *J. Geophys. Res.*, *94*, 9251-9274, 1989.

Juteau, T., J. P. Eisson, J. Franchteau, H. D. Needham, P. Choukroune, C. Rangin, M. Sequret, R. O. Ballard, P. J. Fox, W. R. Normark, A. Garramza, D. Cordoba, and J. Guerreo, Homogeneous basalts from the East Pacific Rise at 21°N: Steady state magma reservoirs at moderately fast spreading centers, *Oceanol. Acta*, *3*, 487-503, 1980.

Karsten, J. L., Spatial and temporal variations in the petrology, morphology and tectonics of a migrating spreading center: The Endeavor Segment, Juan de Fuca Ridge, Ph. D. thesis, 349 pp., Univ. of Wash., Seattle, 1988.

Karsten, J. L., J. R. Delaney, J. M. Rhodes, and R. A. Lilias, Spatial and temporal evolution of magmatic systems beneath the endeavour segment, Juan de Fuca ridge: Tectonic and petrologic constraints, *J. Geophys. Res.*, *95*, 19,235-19,256, 1990.

Kelemen, P. B., Reaction between ultramafic rock and fractionating basaltic magma, I, phase relations, the origin of calc-alkaline magma series, and the formation of discordant dunite, *J. Petrol.*, *31*, 51-98, 1990.

Kelemen, P. B., D. M. Joyce, J. D. Webster, and J. R. Holloway, Reaction between ultramafic rock and fractionating basaltic magma, II, Experimental investigations of reaction between olivine tholeiite and harzburgite at 1150-1050°C and 5 kb, *J. Petrol.*, *31*, 99-134, 1990.

Kelemen, P. B., H. J. B. Dick, and J. E. Quick, Formation of harzburgite by pervasive melt/rock reaction in the upper mantle, *Nature*, *358*, 635-641, 1992.

Kinzler, R. J., and T. L. Grove, Primary magmas of mid-ocean ridges basalts, 2, Applications, *J. Geophys. Res.*, *97*, 6907-6926, 1992.

Klein, E. M., and C. L. Langmuir, Global correlations of ocean ridge basalt chemistry with axial depth and crustal thickness, *J. Geophys. Res*, *92*, 8089-8115, 1987.

Klein, E. M., and C. H. Langmuir, Local versus global variation in ocean ridge basaltic composition: A reply, *J. Geophys. Res.*, *94*, 4241-4252, 1989.

Klein, E. M., C. H. Langmuir, H. Staudigel, Geochemistry of basalts from the Southeast Indian ridge, 115°E-138°E, *J. Geophys. Res.*, *96*, 2089-2107, 1991.

Kuo, B.-Y., and D. W. Forsyth, Gravity anomalies of the ridge transform system in the south Atlantic between 31° and 34.5°S: Upwelling centers and variations in crustal thickness, *Mar. Geophys. Res.*, *10*, *205-232*, 1988.

Langmuir, C. H., J. F. Bender, A. B. Bence, and G. N. Hanson, Petrogenesis of basalts from the FAMOUS area: Mid-Atlantic Ridge, *Earth Planet. Sci. Lett.*, *36*, 133-156, 1977.

Langmuir, C. H., J. F. Bender, and R. Batiza, Petrological and tectonic segmentation of the East Pacific Rise, 5°30'-14°30', *Nature*, *322*, 422-429, 1986.

Le Roex, A. P., H. J. B. Dick, A. M. Reid, and A. L. Erlank, Ferrobasalts from the Speiss Ridge segment of the Southwest Indian Ridge, *Earth Planet. Sci. Lett.*, *60*, 437-451, 1982.

Le Roex, A. P., H. J. B. Dick, A. L. Erlank, A. M. Reid, F. A. Frey, and S. R. Hart, Geochemistry, mineralogy and petrogenesis of lavas erupted along the Southwest Indian Ridge between the Bouvet Triple Junction and 11 degrees east, *J. Petrol.*, *24*, 267-318, 1983.

Le Roex, A. P., H. J. B. Dick, A. L. Erlank, A. M. Reid, F. A. Frey, and S. R. Hart, Petrology and geochemistry of basalts from the American-Antarctic Ridge, southern ocean: Implications for the westward influence of the Bouvet mantle plume, *Contrib. Mineral. Petrol.*, *90*, 367-380, 1985.

Le Roex, A. P., H. J. B. Dick, L. Gulen, A. M. Reid, and A. J. Erlank, Local and regional heterogeneity in MORB from the Mid-Atlantic Ridge between 54.5°S and 51°S: Evidence for geochemical enrichment, *Geochim. Cosmochim. Acta*, *51*, 541-555, 1987.

Lin, J., and J. Phipps Morgan, The spreading rate dependance of three-dimensional mid-ocean ridge gravity structure, *Geophy. Res. Lett.*, *19*, 13-16, 1992.

Lin, J., G. M. Purdy, H. Schouten, J.-C. Sempere, and C. Zervas, Evidence from gravity data for focused magmatic accretion along the Mid-Atlantic Ridge, *Nature*, *344*, 627-632, 1990.

Macdonald, K. C., Mid-ocean ridges: Fine scale tectonic, volcanic, and hydrothermal processes within the plate boundary zone, *Annu. Rev. Earth Planet. Sci.*, *10*, 155-190, 1982.

Macdonald, K. C., P. J. Fox, L. J. Perram, M. F. Eisen, R. M. Haymon, S. P. Miller, S. M. Carbotte, M.-H. Cormier, and A. M. Shor, A new view of the mid-ocean ridge from the behavior of ridge-axis discontinuities, *Nature*, *335*, 217-225, 1988.

Malinverno, A., Inverse square-root dependance of mid-ocean ridge

flank roughness on spreading rate, *Nature, 352*, 58-60, 1991.
Malinverno, A., and R. A. Pockalny, Abyssal hill topography as an indicator of episodicity in crustal accretion and deformation, *Earth Planet. Sci. Lett., 99*, 154–169, 1990.
McKenzie, D., The generation and compaction of partially molten rock, *J. Petrol., 25*, 713–765, 1984.
McKenzie, D., and M. J. Bickle, The volume and composition of melt generated by extension of the lithosphere, *J. Petrol., 29*, 625–679, 1988.
Melson, W. G., and T. O'Hearn, "Zero" age variations in the composition of abyssal volcanic rocks along the axial zone of the Mid-Atlantic Ridge, in *The Geology of North America*, vol. M, *The Western North America Region*, edited by P.R. Vogt and B. E. Tucholke, pp. 117-136, Geological Society of America, Boulder, Colo., 1986.
Michael, P. J., R. L. Chase, and J. F. Allan, Petrologic and geologic variations along the southern Explorer ridge, northeast Pacific Ocean, *J. Geophys. Res., 94*, 13,895-13,918, 1989.
Moore, J. G., W. R. Normark, G. R. Hess, and C. E. Meyer, Petrology of basalt from the East Pacific Rise near 21° north latitude, *U.S. Geol. Surv. J. Res., 5-6*, 753-759, 1977.
Morel, J. M., Evolution magmatique le long des dorsales Medio-Atlantique et Est-Pacifique, Ph.D. thesis, Univ. de Bretagne Occidental, 1979.
Morel, J. M., and R. Hekinian, Compositional variation of volcanics along segments of recent spreading ridges, *Contrib. Mineral. Petrol., 72*, 425-436, 1980.
Natland, J. H., Effect of axial magma chambers beneath spreading centers on the compositions of basaltic rocks, *Initial Rep. Deep Sea Drill. Proj., 54*, 833-850, 1980.
Neumann, E. R., and J.-G. Schilling, Petrology of basalts from the Mohns-Knipovich Ridge: The Norwegian-Greenland Sea, *Contrib. Mineral. Petrol., 85*, 209-223, 1984.
Nicolas, A., A melt extraction model based on structural studies in mantle peridotites, *J. Petrol., 27*, 999-1022, 1986.
Niu, Y., Mid-ocean ridge magmatism: Style of mantle upwelling, partial melting, crustal level processes, and spreading rate dependence — A petrologic approach, Ph.D. thesis, Univ. of Hawaii, Honolulu, 250 pp., 1992.
Niu, Y., and Batiza, R., An empirical method for calculating melt compositions produced beneath mid-ocean ridges: Application for axis and off-axis (seamounts) melting, *J. Geophys Res., 96*, 21,753-21,777, 1991*a*.
Niu, Y., and R. Batiza, In-situ densities of MORB melts and residual mantle: Implications for buoyancy forces beneath mid-ocean ridges. *J. Geol., 99*, 767-775, 1991*b*.
O'Hara, M. J., Primary magma and the origin of basalts, *Scott. J. Geol., 1*, 19-40, 1965.
Parmentier, E. M., and J. Phipps Morgan, Spreading rate dependence of three dimensional structure in oceanic spreading centers, *Nature, 348*, 325-328, 1990.
Perfit, M. R., D. J. Fornari, A. Malahoff, and R. W. Embley, Geochemical studies of abyssal lavas recovered by DSRV from Eastern Galapagos Rift, Inca Transform, and Ecuador Rift, 3, Trace element abundances and petrogenesis, *J. Geophys. Res., 88*, 10,551-10,572, 1983.
Phipps Morgan, J., Melt migration beneath mid-ocean ridge spreading centers, *Geophys. Res. Lett., 14*, 1238–1241, 1987.
Qin, Z., Disequilibrium partial melting model and its implications for trace element fractionation during mantle melting, *Earth Planet. Sci. Lett., 112*, 75-90, 1992.
Rabinowicz, M., G. Ceuleneer, and A. Nicolas, Melt segregation and flow in mantle diapirs below spreading centers: Evidence from Oman ophiolite, *J. Geophys. Res., 93*, 429-436, 1987.
Renard, V., R. Hekinian, J. Franchteau, R.D. Ballard, and H. Backer, Submersible observations at the axis of the ultrafast spreading East Pacific Rise (17°S to 21°30'S), *Earth Planet. Sci. Lett., 75*, 339-353, 1985.
Ribe, N. M., Diapirism in the Earth's mantle: Experiments on the motion of a hot sphere in a fluid with temperature - dependent viscosity, *J. Volcanol. Geotherm. Res., 16*, 221-245, 1983.
Schilling, J.-G., R. N. Anderson, and P. R. Vogt, Rare earth, Fe and Ti variations along the Galapagos spreading center and their relationship to the Galapagos mantle plume, *Nature, 261*, 108-112, 1976.
Schilling, J.-G., R. H. Kingsley, and J. D. Devine, Galapagos hot spot spreading system, 1, Spatial, petrological and geochemical variations (83°W-101°W), *J. Geophys. Res., 87*, 5593-5610, 1982.
Schilling, J.-G., M. Zajac, R. Evans, T. Johnston, W. White, J. D. Devine, and R. Kingsley, Petrological and geochemical variations along the Mid-Atlantic Ridge from 29°N to 73°N, *Am. J. Sci., 283*, 510-586, 1983.
Schilling, J.-G., H. Sigurdsson, A. N. Davis, and R. N. Hey, Easter microplate evolution, *Nature, 317*, 325-331, 1985.
Schouten, H., K. D. Klitgord, and J. A. Whitehead, Segmentation of mid-ocean ridges, *Nature, 317*, 225-229, 1985.
Scott, D. R., and D. J. Stevenson, A self-consistent model of melting, magma migration and buoyancy-driven circulation beneath mid-ocean ridges, *J. Geophys. Res., 94*, 2973-2988, 1989.
Sigurdsson, H., First order major element variation in basalt glasses from the Mid-Atlantic Ridge: 29°N to 73°N, *J. Geophys. Res., 86*, 9483-9502, 1981.
Sinton, J. M., and R. S. Detrick, Mid-ocean ridge magma chambers, *J. Geophys. Res., 97*, 197-216, 1992.
Sinton, J. M., S. M. Smaglik, J. J. Mahoney, and K. C. Macdonald, Magmatic processes at super fast spreading ridges: glass compositional variations along the EPR 13° - 23°S, *J. Geophys. Res., 96*, 6133-6155, 1991.
Sleep, N. H., Tapping of melts by veins and dikes, *J. Geophys. Res., 93*, 10,255–10,272, 1988.
Small, C., and D. T. Sandwell, An abrupt change in ridge axis gravity with spreading rate, *J. Geophys. Res., 94*, 17,383-17,392, 1989.
Sotin, C., and E. M. Parmentier, Dynamic consequences of compositional and thermal density stratification beneath spreading centers, *Geophys. Res. Let., 16*, , 835-838, 1989.
Stakes, D. S., J. W. Shervais, and C. A. Hopson, The volcanic-tectonic cycle of the FAMOUS and AMAR valleys, Mid-Atlantic Ridge (36°47'N): Evidence from basalt glass and phenocryst compositional variations for a steady-state magma chamber beneath valley midsections, AMAR 3, *J. Geophys. Res., 89*, 6995-7028, 1984.
Stolper, E., A phase diagram for mid-ocean ridge basalts: Preliminary results and implications for petrogenesis, *Contrib. Mineral. Petrol., 74*, 13-27, 1980.
Thompson, G., W. B. Bryan, and W. G. Melson, Geological and geophysical investigation of the Mid-Cayman Rise spreading center: Geochemical variation and petrogenesis of basalt glasses, *J. Geol., 88*, 41-55, 1980.
Thompson, G., W. B. Bryan, and S. E. Humphris, axial volcanism on the East Pacific Rise, 10° - 12°N, in Magmatism in the Ocean Basin, edited by A. D. Saunders and M. J. Norry, *Geol. Soc. Spec. Publ. London, 42*, 181-200, 1989.
Tighe, S., (Ed.), *East Pacific Rise Data Synthesis*, JOI, Inc., Washington, D. C., 1988.
Whitehead, J. A., H. J. B. Dick, and H. Schouten, A mechanism for magmatic accretion under spreading centers, *Nature, 312*, 146-147, 1984.
Wilson, D. S., Tectonic history of the Juan de Fuca ridge over the last 40 m.y., *J. Geophys. Res., 93*, 11,863-11,876, 1988.

R. Batiza, Department of Geology and Geophysics, University of Hawaii, 2525 Correa Road, Honolulu, HI 96822.
Y. Niu, Lamont-Doherty Earth Observatory, Palisades, NY 10964.

(Received April 3, 1992;
revised November 30, 1992;
accepted January 15, 1993.)